A 3-D Trailer Approach to Leader-Following Formation Control

Pedro Pereira, Rita Cunha, David Cabecinhas, Carlos Silvestre, and Paulo Oliveira

***Abstract*— A real-time 3-D trajectory planner for the leader-following formation control of autonomous vehicles is proposed. The planner relies on the definition of a trailer body whose hinge point is rigidly attached to the leader and assigns each follower to a distinct point of such a trailer. Convergence results for the trailer body reference frame are presented based on Lyapunov analysis, which guarantee that the planning can be independently implemented by n followers, with a common leader, as they asymptotically behave as n points of a unique trailer body. As such, the need for communication among followers is dispensable. The proposed strategy is divided into trajectory planning and trajectory tracking, the first problem being vehicle-independent. Experimental results obtained with quadrotor vehicles are presented, which demonstrate the richness and suitability of the planned trajectories.**

***Index Terms*— Motion planning, path planning, nonlinear control systems, unmanned aerial vehicles.**

I. Introduction

CONTROL of multi-vehicle systems is an active research topic thanks to the benefits to be gained by adequately exploring the capabilities of a group of mobile robots. For instance, multiple robots are essential in load transportation where payload limitations inherent to a single vehicle may be overcome with a properly sized group of vehicles [1], [2]. Multi-robot systems prove also useful in mapping, covering, and surveillance of large areas, such as the sea floor [3], [4], or in implementing distributed and reconfigurable sensor networks [5]. The completion of such tasks depends greatly on the geometric pattern between the group of vehicles or equivalently on the group formation.

Different approaches to formation control have been proposed in the literature. In a behavior-based approach, a desired behavior results from a weighting between different goal-oriented behaviors [6]–[9]. It can be implemented in a decentralized manner, thus requiring reduced information exchange among vehicles, but it proves difficult to guarantee convergence to the desired formation. In a virtual structure approach [10]–[13], the vehicles move as points of a virtual rigid body, whose motion is prescribed in a global manner, thus requiring full cooperation between all vehicles.

The leader-following strategy is a third approach to formation control and it has been extensively studied, particularly in a 2-D setting [14]–[23]. The goal of a leader-following approach may be defined as having each follower vehicle at a fixed position relative to the leader, whose motion is independent of that of the followers'. The problem is completely characterized by the relative position vector and the reference frame where it is defined and, not unexpectedly, the choice of such a reference frame plays a crucial role in the definition of the follower's trajectory and in the sensory information necessary for computing such a trajectory.

The simplest approach in a leader-following strategy is to specify the relative position vector in the inertial reference frame as in [5] and [22]. This method results in a simple trajectory for the follower, in the sense that both the leader and the follower describe an identical path, apart from a translation. Since the leader may describe an arbitrary motion, then it is possible for the leader and the follower to track the same path, which happens when the leader moves along the relative position vector direction, thus reducing the efficiency gains of using multiple vehicles. A more evolved formation control strategy is proposed in [24] and [25], where attractive and repulsive interactions are designed such that a certain intervehicle spacing is attained. However, the resulting vehicles' configuration is not unique in the sense that it depends on the initialization of the formation.

Another alternative, proposed by several authors [15], [16], [18], [19], defines the relative position vector in a reference frame attached to the leader, namely the leader's Frenet reference frame. For this choice, the follower describes trajectories

Manuscript received April 2, 2018; revised July 1, 2019; accepted August 12, 2019. Date of publication September 20, 2019; date of current version October 9, 2020. Manuscript received in final form August 28, 2019. This work was supported in part by the Macau Science and Technology through the Development Fund under Grant FDCT/026/2017/A1, in part by the Projects of University of Macau under Grant MYRG2018-00198-FST and Grant MYRG2016-00097-FST, in part by the Fundação para a Ciência e a Tecnologia (FCT) through the Institute for Systems and Robotics (ISR) under Contract LARSyS UID/EEA/50009/2019 and through the Mechanical Engineering Institute (IDMEC) under Contract LAETA UID/EMS/50022/2019, and in part by the EU Horizon 2020 Research and Innovation Programme (MULTIDRONE) under Grant 731667. Recommended by Associate Editor Y. Ebihara. *(Corresponding author: Pedro Pereira.)*

P. Pereira is with the Automatic Control Department, KTH Royal Institute of Technology, 114 28 Stockholm, Sweden (e-mail: ppereira@kth.se).

R. Cunha is with the Institute for Robotics and Systems in Engineering and Science (LARSyS), Instituto Superior Técnico, Universidade de Lisboa, 1049-001 Lisbon, Portugal, and also with the Department of Electrical Engineering and Computer Science, Instituto Superior Técnico, Universidade de Lisboa, 1049-001 Lisbon, Portugal (e-mail: rita@isr.ist.utl.pt).

D. Cabecinhas and C. Silvestre are with the Institute for Robotics and Systems in Engineering and Science (LARSyS), Instituto Superior Técnico, Universidade de Lisboa, 1049-001 Lisbon, Portugal, and also with the Department of Electrical and Computer Engineering, Faculty of Science and Technology, University of Macau, Macau, China (e-mail: dcabecinhas@isr.ist.utl.pt; cjs@isr.ist.utl.pt).

P. Oliveira is with the Institute for Robotics and Systems in Engineering and Science (LARSyS), Instituto Superior Técnico, Universidade de Lisboa, 1049-001 Lisbon, Portugal, and also with the Department of Mechanical Engineering, Instituto Superior Técnico, Universidade de Lisboa, 1049-001 Lisbon, Portugal (e-mail: pjcro@isr.ist.utl.pt).

Color versions of one or more of the figures in this article are available online at http://ieeexplore.ieee.org.

Digital Object Identifier 10.1109/TCST.2019.2939119

that are not a mere offset of the leader's, but it requires a larger control effort [26]. In particular, at the kinematic level, the explicit knowledge of parameters that are not easily measured or estimated by the follower, such as the leader's reference frame angular velocity, is required when computing the desired trajectory. Additionally and more importantly, the works deal with a 2-D setting and an extension for a 3-D environment is not trivial, as a unique and continuous reference frame attached to the leader does not exist.

Finally, another alternative is to define the relative position vector in a frame attached to a *virtual* follower vehicle, similar to [14] and [21], and imposing some constraints on its motion. In this article, a similar but novel approach is followed, where one considers a *virtual* follower body as a 3-D trailer attached to the leader via a longitudinal link. This article shows that the trailer reference frame has an asymptotically stable configuration. Thus, one can imagine n followers whose desired position is prescribed as the position of n distinct points within their own trailer reference frame and, for the proposed trajectory planner, they asymptotically behave as n points of a unique trailer reference frame.

The proposed strategy shares similarities with the virtual structure approach: in a virtual structure approach, the vehicles move as points of a virtual rigid body, whose motion is prescribed in a global manner. In our approach, there is no virtual rigid body: the leader is a real vehicle, and it provides, in a sense, a global vehicle (i.e., all followers must follow the same leader); moreover, the followers do not need to agree on the leader's motion (the leader moves independently of the followers), while in the methods based on a virtual structure, all followers must decide *a priori* on the virtual rigid body motion. In addition, our approach also requires less sensory information than the strategies based on the leader Frenet reference frame [15], [16], [18], [19], particularly at the kinematic level, where only the knowledge of the leader linear velocity is required.

As opposed to an ideal vehicle that tracks with infinite precision the planned trajectory, the real follower vehicle cannot change its position instantaneously, which means it does not necessarily start or remain at a specific relative distance with respect to the leader. With that in mind, a two part solution to the leader-follower formation problem is proposed. First, a desired trajectory is computed for an ideal follower vehicle, hereafter called *virtual* follower, which keeps a constant distance to the leader at all times. This reference trajectory is then used as a reference to a trajectory-tracking controller that drives the *real* follower vehicle to the desired trajectory. In this article, we focus on the first problem of generating the follower trajectory and present experimental results for the complete planning and tracking problem using quadrotor vehicles. Note that the planning is executed on the fly, meaning that the trajectory of the virtual follower is computed as the leader progresses and no *a priori* knowledge of the leader's trajectory is required.

Quadrotors are aerial vehicles ideal for testing algorithms, due to their simplicity, high maneuverability, vertical take-off/landing, and hover capability and ability to track any trajectory within the limits of their actuation dynamics. Tracking controllers for quadrotor vehicles have been extensively studied in the literature, see the survey article [27], and the *virtual* follower trajectory generated by our planner can be used as a reference for any generic tracking controller applied to the follower vehicle.

In summary, the trailer approach proposed in this article provides a follower trajectory planner that, despite its simplicity (when compared, for example, with approaches based on the leader's Frenet frame [15], [16], [18], [19]), is able to produce follower trajectories that are not mere copies of the leader's trajectories and that are intuitive, in the sense that the followers asymptotically evolve as points on a unique trailer attached to the leader. As opposed to the artificial potential fields approach [24], this asymptotic behavior is uniquely defined, meaning that it does not depend on the initial conditions. Moreover, formal guarantees of convergence with wide and explicitly defined regions of attraction are provided, which is lacking from the behavior-based approach [6] and guaranteed locally for artificial potential fields.

The remainder of this article is structured as follows. Section II presents the mathematical notation used throughout this article. Section III describes the leader–follower problem and Section IV describes the proposed trajectory planner. Section V summarizes the main results and contributions. Section VI presents the trajectory planner equations of motion and Sections VII and VIII analyze the trajectory planner properties. Section IX describes the experimental setup for the quadrotor vehicles and presents the obtained experimental results. A preliminary and reduced version of this article was published in the 2014 IEEE International Conference on Robotics and Automation [28]. With respect to the preliminary version, this article presents significantly more details on the derivation of the main theorems and provides additional results. In particular, the proposed solution is analyzed for robustness to measurement noise and a discussion is added on the dual problem of fixing the followers' motion rather than that of the leader.

II. Notation

The configuration of a reference frame $\{B\}$ with reference to a frame $\{A\}$ is represented as an element of the Special Euclidean group, $({}^{\mathcal{A}}_{\mathcal{B}}\mathcal{R}, {}^{\mathcal{A}}\mathbf{p}_{\mathcal{B}}) \in \mathcal{SE}(3)$, where ${}^{\mathcal{A}}\mathbf{p}_{\mathcal{B}} \in \mathbb{R}^3$ is the position and ${}^{\mathcal{A}}_{\mathcal{B}}\mathcal{R} \in \mathcal{SO}(3)$ is the rotation matrix. For points in the inertial frame $\{\mathcal{I}\}$, the superscript letter is often omitted, i.e., $\mathbf{p}_{\mathcal{B}} := {}^{\mathcal{I}}\mathbf{p}_{\mathcal{B}}$. A point velocity vector is denoted by $\mathbf{v}_s$ when specified in the inertial reference frame, and denoted by $\mathbf{u}_s$ when specified in the reference attached to the point (both appended with a meaningful subscript s). The following functions and symbols are used throughout this article. The sign function $\text{sign} : \mathbb{R} \to \{-1, 0, 1\}$ satisfies $\text{sign}(0) = 0$ and $\text{sign}(x) = x|x|^{-1}$ for $x \neq 0$. The map $S : \mathbb{R}^3 \to \mathbb{R}^{3\times 3}$ yields a cross-product skew-symmetric matrix such that $S(\mathbf{a})\mathbf{b} = \mathbf{a} \times \mathbf{b}$ for all $\mathbf{a}, \mathbf{b} \in \mathbb{R}^3$. The map $\Pi : \{\mathbf{x} \in \mathbb{R}^3 : \mathbf{x}^T\mathbf{x} = 1\} \to \mathbb{R}^{3\times 3}$, where $\Pi(\mathbf{x}) = S^T(\mathbf{x})S(\mathbf{x})$ yields a matrix that represents the orthogonal projection operator onto the subspace perpendicular to $\mathbf{x}$. The vectors $\mathbf{e}_i \in \mathbb{R}^3$ with $i = \{1, 2, 3\}$ denote the canonical basis unit vectors in $\mathbb{R}^3$. We

write as $\mathbf{f}^{(i)}(t)$ the ith time derivative of $\mathbf{f} : \mathbb{R}_{\geq 0} \to \mathbb{R}^n$ for $i = \{1, 2, \dots\}$.

III. Problem Statement

In a leader-following strategy, it is the *goal* of a follower vehicle to move so as to remain and to *see* a leader vehicle at a specified constant distance. The leader vehicle moves freely and independently of its follower, so our focus lies on planning follower trajectories that achieve the leader-following goal previously described. Accomplishing this goal relies on the definition of an ideal follower vehicle that is kept at a constant distance to the leader (not necessarily along a constant direction), which is named hereafter a *virtual* follower.

Consider the inertial reference frame $\{\mathcal{I}\} \in \mathcal{SE}(3)$, the leader's Frenet reference frame $\{\mathcal{L}\}$ defined by the pair $({}^{\mathcal{I}}_{\mathcal{L}}\mathcal{R}, \mathbf{p}_{\mathcal{L}}) \in \mathcal{SE}(3)$, and the *virtual* follower reference frame $\{\mathcal{F}\}$ defined by the pair $({}^{\mathcal{I}}_{\mathcal{F}}\mathcal{R}, \mathbf{p}_{\mathcal{F}}) \in \mathcal{SE}(3)$. The kinematics of the leader are given by

$$\begin{aligned} \dot{\mathbf{p}}_{\mathcal{L}}(t) &= \mathbf{v}_{\mathcal{L}}(t) \equiv {}^{\mathcal{I}}_{\mathcal{L}}\mathcal{R}(t)\mathbf{u}_{\mathcal{L}}(t) \\ {}^{\mathcal{I}}_{\mathcal{L}}\dot{\mathcal{R}}(t) &= {}^{\mathcal{I}}_{\mathcal{L}}\mathcal{R}(t)\mathcal{S}\left(\boldsymbol{\omega}_{\mathcal{L}}(t)\right) \end{aligned} \tag{1}$$

where $\mathbf{v}_{\mathcal{L}} : \mathbb{R}_0 \to \mathbb{R}^3$ is the linear velocity expressed in inertial coordinates; $\mathbf{u}_{\mathcal{L}}(t) = \|\mathbf{v}_{\mathcal{L}}(t)\|\mathbf{e}_1$, since $\{\mathcal{L}\}$ is a Frenet reference frame; and $\boldsymbol{\omega}_{\mathcal{L}} : \mathbb{R}_0 \to \mathbb{R}^3$ is the angular velocity of the leader's Frenet reference frame. For the sake of simplicity, the leader vehicle speed is hereafter denoted by $v_{\mathcal{L}}(t) := \|\mathbf{v}_{\mathcal{L}}(t)\|$. Using the path curvature $\kappa_{\mathcal{L}}$ and path torsion $\tau_{\mathcal{L}}$, the leader's angular velocity may be written as

$$\boldsymbol{\omega}_{\mathcal{L}}(t) = v_{\mathcal{L}}(t)\begin{bmatrix}\tau_{\mathcal{L}}(t) & 0 & \kappa_{\mathcal{L}}(t)\end{bmatrix}^T =: v_{\mathcal{L}}(t)\boldsymbol{\kappa}_{\mathcal{L}}(t)$$

where $\boldsymbol{\kappa}_{\mathcal{L}} : \mathbb{R}_{\geq 0} \to \Omega_{\boldsymbol{\kappa}}$ with $\Omega_{\boldsymbol{\kappa}} := \{(\tau_{\mathcal{L}}, 0, \kappa_{\mathcal{L}}) \in \mathbb{R} \times \mathbb{R} \times \mathbb{R}_{\geq 0}\} \backslash \{(\tau_{\mathcal{L}}, 0, \kappa_{\mathcal{L}}) \in \mathbb{R}^3 : \kappa_{\mathcal{L}} = 0 \wedge \tau_{\mathcal{L}} \neq 0\}$. We observe that the path curvature is always nonnegative and that the path torsion is not defined when the path curvature is zero, which is the reason for introducing the set $\Omega_{\boldsymbol{\kappa}}$. The kinematics of the follower reference frame are similarly defined.

Definition 1: Given a distance $\mathrm{d} > 0$ and a unit vector $\mathbf{n}$, the leader-following goal is accomplished when a *virtual* follower remains at a fixed relative position with respect to the leader from its own point of view, such that, for all $t \geq 0$

$${}^{\mathcal{F}}\mathbf{p}_{\mathcal{L}|\mathcal{F}}(t) := {}^{\mathcal{F}}_{\mathcal{I}}\mathcal{R}(t)(\mathbf{p}_{\mathcal{L}}(t) - \mathbf{p}_{\mathcal{F}}(t)) = \mathrm{d}\mathbf{n}. \tag{2}$$

The planning challenge lies in finding a time evolution for $t \mapsto {}^{\mathcal{I}}_{\mathcal{F}}\mathcal{R}(t)$, given an initial condition ${}^{\mathcal{I}}_{\mathcal{F}}\mathcal{R}(0)$, such that the follower describes a path that is not a mere offset of the leader's path but is instead an intuitive motion when compared with the leader's. Note that, given $t \mapsto {}^{\mathcal{I}}_{\mathcal{F}}\mathcal{R}(t)$, a unique solution $t \mapsto \mathbf{p}_{\mathcal{F}}(t)$ exists, which satisfies (2), meaning that defining the time evolution of $t \mapsto {}^{\mathcal{I}}_{\mathcal{F}}\mathcal{R}(t)$ or, equivalently, defining the angular velocity $t \mapsto \boldsymbol{\omega}_{\mathcal{F}}(t)$, given an initial condition ${}^{\mathcal{I}}_{\mathcal{F}}\mathcal{R}(0)$, completely solves the planning problem. In addition, note that there exists an infinite number of reference frames $t \mapsto {}^{\mathcal{F}}_{\mathcal{I}}\mathcal{R}(t)$ that satisfy $t \mapsto \|\mathbf{p}_{\mathcal{L}}(t) - \mathbf{p}_{\mathcal{F}}(t)\| = d$. However, apart from a rotation around the first axis, only one rotation matrix $t \mapsto {}^{\mathcal{F}}_{\mathcal{I}}\mathcal{R}(t)$ exists that guarantees simultaneously that $\mathbf{n} = \mathbf{e}_1$. This choice of frame proves more convenient regarding the analysis of the planner's behavior. Furthermore, choosing some other frame that satisfies (2) does not have any impact on the planned trajectory, for example, if one sees a leader ahead and it moves straight, it is exactly the same as one seeing a leader at a right angle but now moving sideways, the only difference being a 90° rotation.

Note that the *virtual* follower's position, $t \mapsto \mathbf{p}_{\mathcal{F}}(t)$, does not necessarily match the *real* follower's position. Thus, a two-step approach for solving the leader-following problem is proposed: first, a trajectory-planning problem and, second, a trajectory-tracking problem. For the trajectory-planning problem, a *virtual* vehicle is designed, where (2) is always met. The planning problem is vehicle-independent, so, for example, it does not depend on the mass of the *real* follower vehicle. For the trajectory-tracking problem, a controller is designed, which guarantees that the *real* follower's position tracks the *virtual* follower's position, with whatever position error existing being steered to zero. This problem is vehicle-dependent, depending, for example, on the actuation limits of the *real* follower vehicle.

The combined problem of planning and tracking a trajectory for leader following is complex in the sense that a planned trajectory may not be feasible for the vehicle. When $t \mapsto \boldsymbol{\omega}_{\mathcal{F}}(t) = \mathbf{0}$ (in this case, $t \mapsto {}^{\mathcal{I}}_{\mathcal{F}}\mathcal{R}(t)$ is constant) or when $d = 0$, the follower mimics the leader, with and without an offset, respectively, in which case feasibility of the planned trajectory depends exclusively on the leader's trajectory feasibility (assuming that the leader vehicle and the *real* follower vehicle are identical). By continuity, if the leader is not close to the limits of its flight envelope, then the same conclusion extends to the followers, as long as $t \mapsto \|\boldsymbol{\omega}_{\mathcal{F}}(t)\|$ or d are sufficiently small. We emphasize that, in order to not collide with the leader, d should not be *small*, which means the final planning should strive to obtain a *small* $t \mapsto \|\boldsymbol{\omega}_{\mathcal{F}}(t)\|$.

This article focuses almost exclusively on the trajectory planning. The trajectory planning proposed here is to be implemented for n followers with one common leader. The objective is for the $n + 1$ vehicles to move in a cohesive manner, i.e., to move in a fixed configuration with respect to some known reference frame. However, in order to minimize communications among vehicles, we require each follower to move independently of its peers, i.e., to follow the leader regardless of whether the other vehicles do the same. Under certain conditions, we guarantee that the $n + 1$ vehicles asymptotically move in a fixed formation, with geometry determined by some prespecified distance vectors $\bar{\mathbf{d}}$ (one for each follower). In summary, the trajectory-planning problem is stated as follows.

Problem 1: Given a leader vehicle with kinematics described by (1) and n *virtual* follower vehicles, define the kinematics of each follower independently and based solely on the leader's position and velocity expressed in the *virtual* follower's reference frame, such that the leader-following goal (2) is satisfied at all times and for all followers and such that the $n + 1$ vehicles asymptotically move in a fixed formation.

IV. Trajectory Planner

As previously discussed, the *virtual* follower position is completely defined once the kinematics of the follower's

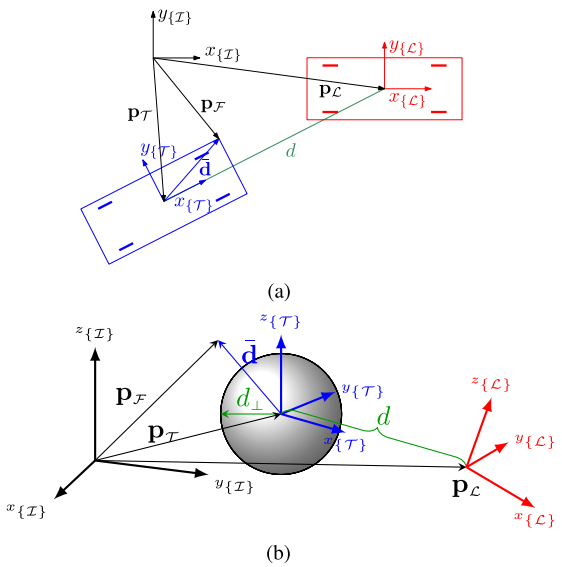

Fig. 1. 3-D trailer with hinge point rigidly connected to the leader by a rod of length d along the longitudinal axis. (a) 2-D trailer. (b) 3-D trailer (generalization of 2-D trailer, illustrated above).

rotation matrix have been set. By selecting an appropriate $t \mapsto \boldsymbol{\omega}_{\mathcal{F}}(t)$, one can generate interesting trajectories that are not simple offsets and which behave in an natural manner according to the leader's motion.

For example, if one chooses $t \mapsto \boldsymbol{\omega}_{\mathcal{F}}(t) = 0$, then the *virtual* follower vehicle follows the leader's path with an offset given by ${}^{\mathcal{I}}_{\mathcal{F}}\mathcal{R}(t)\mathbf{d}$, where ${}^{\mathcal{I}}_{\mathcal{F}}\mathcal{R}(t) = {}^{\mathcal{I}}_{\mathcal{F}}\mathcal{R}(0)$ for all $t \geq 0$. Take another example where the leader stays at rest and where $t \mapsto \boldsymbol{\omega}_{\mathcal{F}}(t) = \boldsymbol{\omega}$ with ${}^{\mathcal{I}}_{\mathcal{F}}\mathcal{R}(0)\mathbf{e}_3 = (\boldsymbol{\omega}/\|\boldsymbol{\omega}\|)$ and for some $\boldsymbol{\omega} \in \mathbb{R}^3\backslash\{\mathbf{0}\}$; in that case, the *virtual* follower rotates around the leader and about the axis $(\boldsymbol{\omega}/\|\boldsymbol{\omega}\|)$. These are two types of uninteresting *virtual* followers.

In this section, we propose an interesting follower behavior, which is also intuitive in the sense that the *virtual* follower is modeled as a point of a 3-D trailer reference frame $\{\mathcal{T}\}$, with hinge point $\mathbf{p}_{\mathcal{T}}$ and orientation ${}^{\mathcal{I}}_{\mathcal{T}}\mathcal{R} \equiv {}^{\mathcal{I}}_{\mathcal{F}}\mathcal{R}$. The trailer hinge point is rigidly attached to the leader vehicle by a longitudinal rigid link of length d, as shown in Fig. 1 [which shows a 3-D trailer in Fig. 1(b) as a generalization of a 2-D trailer in Fig. 1(a)]. If this link behaves as a trailer link, then an intuitive *virtual* follower is obtained, where the longitudinal direction, or ${}^{\mathcal{I}}_{\mathcal{T}}\mathcal{R}\mathbf{e}_1$, is controlled by the pitch and the yaw angular rates. Second, a roll angular rate is designed, such that the orthogonal space to the longitudinal direction has a stable equilibrium solution. For the roll rate design, a new distance $d_\perp$ is introduced, which can be viewed as the radius of a spherical trailer. This idea is shown in Fig. 1.

Modeling the *virtual* follower as a point in a 3-D trailer reference frame $\{\mathcal{T}\}$ is equivalent to having

$$\mathbf{p}_{\mathcal{F}}(t) = \mathbf{p}_{\mathcal{T}}(t) + {}^{\mathcal{I}}_{\mathcal{T}}\mathcal{R}(t)\bar{\mathbf{d}}(t)$$

with $\bar{\mathbf{d}} : \mathbb{R}_{\geq 0} \to \mathbb{R}^3$ as a prespecified distance vector.[1] For a constant $\bar{\mathbf{d}}$, the *virtual* follower moves rigidly with respect to $\{\mathcal{T}\}$ in which case it behaves as a fixed point of a trailer whose volume is not zero. Having a time-varying $\bar{\mathbf{d}}$ adds some degrees of freedom, which may be meaningful in a formation of multiple followers.

Remark 1: The only distances that affect the time evolution of $\{\mathcal{T}\}$ are d and $d_\perp$, which are chosen by the control/system designer. The choice of $\bar{\mathbf{d}} : \mathbb{R}_{\geq 0} \to \mathbb{R}^3$ does not interfere in the time evolution of $\{\mathcal{T}\}$ and, as such, it can be assumed to be the zero function when studying that same reference frame. In fact, all followers must agree on d and $d_\perp$, while each follower must choose a different $\bar{\mathbf{d}}$: asymptotically, the n followers behave as n distinct points of a common trailer reference frame.

A. Studying Convergence of $\{\mathcal{T}\}$

Recalling that each follower moves independently, each with its own trailer reference frame, a natural question that arises is whether the time evolution of $\{\mathcal{T}\}$ is sensitive to its initial condition or perturbations. The following analysis shows that the proposed trajectory planner can be used independently by n follower vehicles, as they asymptotically behave as n points of a common trailer reference frame.

When studying convergence of $\{\mathcal{T}\}$, the leader Frenet reference frame is the most natural choice: it is uniquely defined (so it poses no ambiguity issues) and also the motion of the *virtual* follower is attached to the motion of the leader, which is encoded in the leader's frame. Thus, the leader-following goal (2) may be rewritten as

$$ {}^{\mathcal{L}}\mathbf{p}_{\mathcal{L}|\mathcal{T}}(t) = d\,{}^{\mathcal{L}}_{\mathcal{T}}\mathcal{R}(t)\mathbf{e}_1 \tag{3}$$

where $t \mapsto {}^{\mathcal{L}}_{\mathcal{T}}\mathcal{R}(t) := {}^{\mathcal{L}}_{\mathcal{I}}\mathcal{R}(t){}^{\mathcal{I}}_{\mathcal{T}}\mathcal{R}(t)$ is the rotation matrix from $\{\mathcal{T}\}$ to $\{\mathcal{L}\}$. There are two types of leaders, one with $t \mapsto {}^{\mathcal{I}}_{\mathcal{L}}\mathcal{R}(t)$, well defined for all times, and another with $t \mapsto {}^{\mathcal{I}}_{\mathcal{L}}\mathcal{R}(t)\mathbf{e}_1$, well defined for all times [a discontinuity in $t \mapsto {}^{\mathcal{I}}_{\mathcal{L}}\mathcal{R}(t)$ corresponds to a reinitialization of our planning algorithm (see [29, Remark 5])].

Proposition 1: If $\mathbf{v}_{\mathcal{L}} : \mathbb{R}_{\geq 0} \to \mathbb{R}^3$ is continuously differentiable and $\|\mathbf{v}_{\mathcal{L}}(t)\| \geq v_{\mathcal{L}}^{\min} > 0$ for all $t \geq 0$, then ${}^{\mathcal{I}}_{\mathcal{L}}\mathcal{R}(t)\mathbf{e}_1$ is well defined for all $t \geq 0$. In addition, if $\|\mathcal{S}\left(\dot{\mathbf{v}}_{\mathcal{L}}(t)\right)\mathbf{v}_{\mathcal{L}}(t)\| \neq 0$, then ${}^{\mathcal{I}}_{\mathcal{L}}\mathcal{R}(t)$ is also well defined, for all $t \geq 0$.

In addition, the planned path depends on the leader's path curvature and torsion, which is the motivation for introducing Definition 2.

Definition 2: A trimming path is the one where the path curvature, κ, and path torsion, τ, are constant throughout the path (i.e., any helix, circular, or rectilinear path is a trimming path). All other paths are called nontrimming.

V. Summary of Main Results

In this section, we summarize our main results and contributions. Given an upper bound on the leader's path curvature (or equivalently, given a lower bound on the path radius), the following holds.

1) For a leader describing a trimming path, the trailer's trajectory has an almost global asymptotically stable (AGAS) and locally exponentially stable equilibrium solution, as well as an unstable equilibrium solution, both analytically determined (Theorem 1).

[1]The trailer orientation can be thought to be identical to the *virtual* follower orientation, i.e., ${}^{\mathcal{I}}_{\mathcal{T}}\mathcal{R} \equiv {}^{\mathcal{I}}_{\mathcal{F}}\mathcal{R}$; in fact, the only difference between the trailer reference frame and the *virtual* follower reference frame is an offset $\bar{\mathbf{d}}$.

2) For a leader describing a nontrimming path, the trailer's trajectory has an exponentially stable solution (analytically undetermined) and convergence is guaranteed, given a proper initialization (Theorem 2).
3) The trailer's trajectory is input to state stable with respect to noisy velocity measurements (Theorem 4).

We point out that the trailer motion is actually completely defined by $t \mapsto {}^{\mathcal{I}}_{\mathcal{T}}\mathcal{R}(t)\mathbf{e}_1$, as shown later. As such, all the stability properties mentioned above for the trailer trajectory are necessarily those of $t \mapsto {}^{\mathcal{I}}_{\mathcal{T}}\mathcal{R}(t)\mathbf{e}_1$. For the convergence of the orthogonal space to $t \mapsto {}^{\mathcal{I}}_{\mathcal{T}}\mathcal{R}(t)\mathbf{e}_1$, we also draw some conclusions. Namely, given an upper bound on the leader's path torsion, the following holds.

1) For a leader describing a trimming path, the trailer's rotation matrix $t \mapsto {}^{\mathcal{I}}_{\mathcal{T}}\mathcal{R}(t)$ has an asymptotically stable equilibrium solution and three unstable equilibrium solutions, with all solutions analytically determined (Theorem 5).
2) For a leader describing a nontrimming path, the trailer's rotation matrix has an asymptotically stable equilibrium solution, analytically undetermined (Theorem 6).

The upper bounds on the leader path curvature and torsion depend on the choice of d and $d_\perp$ and they should not be understood as limitations. Given any leader's path, we can always choose a sufficiently large *distance*, so that the motion of the leader along that path is perceived, as the leader stays at rest. In such a situation, the ideal behavior is for the follower to remain at rest, which is exactly what is obtained with the proposed strategy. A *small* path is associated with a large curvature and/or torsion, while the *distance* is a parameter that must be specified by the designer. The distance d is primarily associated with the leader curvature (and $d_\perp$ with the torsion) so that if the leader describes a path with a radius much smaller than d, the follower stays almost at rest. Thus, d and $d_\perp$ may be selected as sensitivity parameters, i.e., they encode how sensitive the followers are to the leader's motion, which is in agreement with the intuitive behavior that is expected from a trailer system.

VI. 3-D Trailer

As mentioned before, in order for the *virtual* follower to move as a point of a trailer attached to the leader, we consider a virtual longitudinal rigid link of length d, i.e., the position of the trailer $\mathbf{p}_{\mathcal{T}} : \mathbb{R}_{\geq 0} \to \mathbb{R}^3$ is defined by

$$\mathbf{p}_{\mathcal{T}}(t) := \mathbf{p}_{\mathcal{L}}(t) - d\,{}^{\mathcal{I}}_{\mathcal{T}}\mathcal{R}(t)\mathbf{e}_1 \tag{4}$$

as shown in Fig. 1. Differentiating (4) yields

$${}^{\mathcal{I}}_{\mathcal{T}}\mathcal{R}(t)\begin{bmatrix}\mathbf{I}_{3\times 3} & \mathcal{S}(-\mathbf{e}_1)\end{bmatrix}\begin{bmatrix}\mathbf{u}_{\mathcal{T}}(t)\\ \boldsymbol{\omega}_{\mathcal{T}}(t)d\end{bmatrix} = \mathbf{v}_{\mathcal{L}}(t) \tag{5}$$

where $\mathbf{u}_{\mathcal{T}} : \mathbb{R}_{\geq 0} \to \mathbb{R}^3$ is the trailer's body-framed velocity and $\boldsymbol{\omega}_{\mathcal{T}} : \mathbb{R}_{\geq 0} \to \mathbb{R}^3$ is the angular velocity of the trailer's rotation matrix ${}^{\mathcal{I}}_{\mathcal{T}}\mathcal{R} : \mathbb{R}_{\geq 0} \to \mathcal{SO}(3)$. In a 3-D setting, a trailer is a vehicle that moves only longitudinally, i.e., $\mathbf{u}_{\mathcal{T}}(t) := u_{\mathcal{T}}(t)\mathbf{e}_1$ for some $u_{\mathcal{T}} : \mathbb{R}_{\geq 0} \to \mathbb{R}$. Solving (5) for $\boldsymbol{\omega}_{\mathcal{T}}(t)$ and $\mathbf{u}_{\mathcal{T}}(t) := u_{\mathcal{T}}(t)\mathbf{e}_1$, it follows that:

$$\begin{aligned}\mathbf{u}_{\mathcal{T}}(t) &= \left(\mathbf{v}_{\mathcal{L}}^T(t)\,{}^{\mathcal{I}}_{\mathcal{T}}\mathcal{R}(t)\mathbf{e}_1\right)\mathbf{e}_1\\ \boldsymbol{\omega}_{\mathcal{T}}(t) &= d^{-1}\mathcal{S}(\mathbf{e}_1)\,{}^{\mathcal{T}}_{\mathcal{I}}\mathcal{R}(t)\mathbf{v}_{\mathcal{L}}(t) + p_{\mathcal{T}}(t)\,\mathbf{e}_1.\end{aligned} \tag{6}$$

Owing to the nature of the longitudinal link, the roll rate $p_{\mathcal{T}} : \mathbb{R}_{\geq 0} \to \mathbb{R}$ is interpreted as a degree of freedom, since it does not affect either $t \mapsto {}^{\mathcal{I}}_{\mathcal{T}}\mathcal{R}(t)\mathbf{e}_1$ or $t \mapsto \mathbf{u}_{\mathcal{T}}(t)$ (if $t \mapsto p_{\mathcal{T}}(t) = 0$, the reference frame $\{\mathcal{T}\} = ({}^{\mathcal{I}}_{\mathcal{T}}\mathcal{R}, \mathbf{p}_{\mathcal{T}})$ is actually a parallel transport reference frame [30]). For now, we neglect the roll rate, but later, in Section VIII-A, it plays an important role in the convergence of the space orthogonal to ${}^{\mathcal{I}}_{\mathcal{T}}\mathcal{R}(\cdot)\mathbf{e}_1$.

The trailer's trajectory is now completely defined by (6). All the variables defined in what follows are used for the purpose of analysis and have no influence on planning in any way. Next, the convergence of the leader–trailer formation is studied: first for a leader describing the trimming paths and afterward for a leader describing the nontrimming paths.

VII. Convergence of the Leader–Trailer Formation

Consider the shorthand notation $\mathcal{R} \equiv {}^{\mathcal{L}}_{\mathcal{T}}\mathcal{R} \equiv \begin{bmatrix}\mathbf{r}_1 & \mathbf{r}_2 & \mathbf{r}_3\end{bmatrix} \equiv [\mathrm{r}_{ij}] \in \mathcal{SO}(3)$, where i and j denote the column and row indices, respectively. The kinematics of $t \mapsto \mathcal{R}(t)$ satisfy

$$\begin{aligned}\dot{\mathcal{R}}(t) &= \mathcal{S}\left({}^{\mathcal{L}}\boldsymbol{\omega}_{\mathcal{T}|\mathcal{L}}(t)\right)\mathcal{R}(t)\\ &= \mathcal{S}\left(\mathcal{R}(t)\boldsymbol{\omega}_{\mathcal{T}}(t) - \boldsymbol{\omega}_{\mathcal{L}}(t)\right)\mathcal{R}(t).\end{aligned} \tag{7}$$

With this notation, the leader-following goal (3) may be redefined as achieving ${}^{\mathcal{L}}\mathbf{p}_{\mathcal{L}|\mathcal{T}}(t) = d\mathbf{r}_1(t)$, meaning that the relative position between the leader and the trailer is encoded in the vector $t \mapsto \mathbf{r}_1(t) = \mathcal{R}(t)\mathbf{e}_1$. Rotations around $\mathbf{r}_1$ are allowed as they do not break the formation, i.e., all choices for $t \mapsto p_{\mathcal{T}}(t)$ provide the same solution $t \mapsto {}^{\mathcal{L}}\mathbf{p}_{\mathcal{L}|\mathcal{T}}(t)$. The kinematics of $t \mapsto \mathbf{r}_1(t)$, following from (6) and (7), may be written as:

$$\begin{aligned}\dot{\mathbf{r}}_1(t) &= \mathcal{S}\left({}^{\mathcal{L}}\boldsymbol{\omega}_{\mathcal{T}|\mathcal{L}}(t)\right)\mathbf{r}_1(t)\\ &= \frac{v_{\mathcal{L}}(t)}{d}(\Pi(\mathbf{r}_1(t))\mathbf{e}_1 + \mathcal{S}(\mathbf{r}_1(t))\,\kappa_{\mathcal{L}}(t)d)\end{aligned} \tag{8}$$

and additionally the relative angular velocity may be decomposed as ${}^{\mathcal{L}}\boldsymbol{\omega}_{\mathcal{T}|\mathcal{L}} = \Pi(\mathbf{r}_1){}^{\mathcal{L}}\boldsymbol{\omega}_{\mathcal{T}|\mathcal{L}} + \mathbf{r}_1(\mathbf{r}_1^T{}^{\mathcal{L}}\boldsymbol{\omega}_{\mathcal{T}|\mathcal{L}})$. It is worth mentioning that the kinematics of $\mathbf{r}_1$ with respect to the leader arc-length parameterization is autonomous for a leader describing trimming paths and nonautonomous for a leader describing nontrimming paths (see [29, Remark 2]). It also follows that, (8) has an *equilibrium point* for the trimming paths and an *equilibrium trajectory* for the nontrimming paths. Finally, note that $t \mapsto \dot{\mathbf{r}}_1(t)$ is smooth and $t \mapsto \mathbf{r}_1(t)$ belongs to a closed space—the unit sphere, suggesting that at least two equilibrium solutions exist.

A. Pulled Trailer

The unit vector $\mathbf{r}_1$ belongs to the set $\mathcal{S}^2 = \{\mathbf{x} \in \mathbb{R}^3 : \mathbf{x}^T\mathbf{x} = 1\}$, which can be decomposed into three disjoint sets, i.e., $\mathcal{S}^2 = \Omega_1(\epsilon) \cup \Omega_2(\epsilon) \cup \Omega_3(\epsilon)$, where $\Omega_1(\epsilon) = \{\mathbf{x} \in \mathcal{S}^2 : \mathbf{x}^T\mathbf{e}_1 \geq \epsilon\}$, $\Omega_2(\epsilon) = \{\mathbf{x} \in \mathcal{S}^2 : |\mathbf{x}^T\mathbf{e}_1| < \epsilon\}$, and $\Omega_3(\epsilon) = \{\mathbf{x} \in \mathcal{S}^2 : \mathbf{x}^T\mathbf{e}_1 \leq -\epsilon\}$, for some $\epsilon \in (0, 1]$.

Lemma 1: Consider a leader whose path curvature satisfies $(\kappa(t)d)^2 \leq 1-\epsilon^2$ for all $t \geq 0$ and for some $\epsilon \in (0,1]$, and a trailer with kinematics (6). Then, for $\epsilon \neq 1$, $\Omega_1(\epsilon)$ is positively invariant with respect to (8), and for $\mathbf{r}_1(0) \in \Omega_2(\epsilon)$, all the solutions of (8) enter $\Omega_1(\epsilon)$ in finite time. For $\epsilon = 1$ and $\mathbf{r}_1(0) \neq -\mathbf{e}_1$, $t \mapsto \mathbf{r}_1(t)$ converges exponentially fast to $\mathbf{e}_1$.

Proof: From (8), it follows that:

$$\dot{\mathrm{r}}_{11}(t) = v_{\mathcal{L}}(t)d^{-1}\left(1-\mathrm{r}_{11}^2(t)+(\kappa_{\mathcal{L}}(t)d)\mathrm{r}_{12}(t)\right)$$

which is well defined even when r_{12} is ill-defined ($\kappa_{\mathcal{L}}=0$). Consider the nonnegative Lyapunov function $V:[-1,1]\to[0,2]$ defined as $V(\mathrm{r}_{11})=1-\mathrm{r}_{11}$, which is decreasing with r_{11} and $V(\mathrm{r}_{11})=0 \Leftrightarrow \mathrm{r}_{11}=1$. Consider first the case $\epsilon=1$, which implies that $\kappa_{\mathcal{L}}(t)=0$ for all $t\geq 0$. In that case, the Lyapunov time derivative renders

$$\begin{aligned}\dot{V}(\mathrm{r}_{11}(t)) &= -v_{\mathcal{L}}(t)d^{-1}(1+\mathrm{r}_{11}(t))V(\mathrm{r}_{11}(t))\\ &= -v_{\mathcal{L}}(t)d^{-1}(2-V(\mathrm{r}_{11}(t)))V(\mathrm{r}_{11}(t)).\end{aligned}$$

Given that $\mathrm{r}_{11}(0)\neq -1 \Leftrightarrow V(0)\neq 2$, then $t\mapsto V(\mathrm{r}_{11}(t))$ converges exponentially fast to zero and equivalently $t\mapsto \mathbf{r}_1(t)$ converges exponentially fast to $\mathbf{e}_1$. Now consider the case $\epsilon\neq 1$ and suppose $\mathbf{r}_1(t)\in\Omega_2(\epsilon)$ for some finite time interval $t\in[0\ T]$. In that case, $|\mathrm{r}_{11}(t)|<\epsilon \Rightarrow -(1+\epsilon)<-V(\mathrm{r}_{11}(t))$, $|\mathrm{r}_{12}(t)|=(1-(\mathrm{r}_{11}^2(t)+\mathrm{r}_{13}^2(t)))^{1/2}\leq(1-\epsilon^2)^{1/2}$ and $|(\kappa_{\mathcal{L}}(t)d)|<1-\epsilon^2$ for all $t\in[0\ T]$, which means

$$\begin{aligned}\dot{V}(\mathrm{r}_{11}(t)) &\leq -v_{\mathcal{L}}(t)d^{-1}(1-\epsilon)(1-\sqrt{1-\epsilon^2})V(\mathrm{r}_{11}(t))\\ &= -v_{\mathcal{L}}(t)d^{-1}(1-\epsilon^2)(1-\sqrt{1-\epsilon^2}) =: w<0\end{aligned}$$

which is strictly negative for all $t\in[0\ T]$. As such, $[0\ T]\ni t\mapsto V(\mathrm{r}_{11}(t))\leq V(\mathrm{r}_{11}(0))-wt$, which implies that $t\mapsto \mathrm{r}_{11}(t)\geq \mathrm{r}_{11}(0)+wt$. Thus, $t\mapsto\mathbf{r}_1(t)$ leaves the set $\Omega_2(\epsilon)$ and enters the set $\Omega_1(\epsilon)$ in finite time. It also follows that $\Omega_1(\epsilon)$ is positively invariant, since $\dot{V}(\mathrm{r}_{11}(t))<0$ for $\mathrm{r}_{11}(t)=\epsilon$. □

Corollary 1: Consider a leader with path curvature satisfying $(\kappa(t)d)^2\leq(\kappa_{\mathcal{L}}^{\max}d)^2<1$ for all $t\geq 0$, and a trailer with kinematics (6). If $\mathbf{e}_1^T\mathbf{r}_1(0)>0$, then $\mathbf{e}_1^T\mathbf{r}_1(t)>0$ for all $t\geq 0$.

The proof for Corollary 1 consists of considering the limit case of Lemma 1 by taking $\epsilon=0$. Lemma 1 is more general but Corollary 1 is physically more meaningful. It states that $t\mapsto \mathrm{r}_{11}(t)$ is forever positive as long as it is initially positive and as long as $(\kappa_{\mathcal{L}}^{\max}d)^2<1$. It implies that the leader is always in front of the trailer with respect to $\{\mathcal{L}\}$, i.e., $t\mapsto \mathbf{e}_1^{T\,\mathcal{L}}\mathbf{p}_{\mathcal{L}|\mathcal{T}}(t)=d\mathrm{r}_{11}(t)>0$, or, in other words, that the leader is pulling the trailer at all time instants. This result is very general as it applies to both trimming and nontrimming paths. However, despite being applicable to arbitrary paths, it imposes some restrictions on the curvature,[2] specifically that $\kappa_{\mathcal{L}}(t)d<1$ for all $t\geq 0$ (the intuition for this bound is found in [29]).

B. Leader Describing Trimming Paths

Consider a leader describing a path with constant curvature and torsion, i.e., $\dot{\boldsymbol{\kappa}}_{\mathcal{L}}(t)=\mathbf{0}$ for all $t\geq 0$, previously defined as a trimming path. As discussed, rotations around $\mathbf{r}_1$ do not break the formation, which motivates the introduction of the error $\mathbf{z}:\mathcal{S}^2\to\mathbb{R}^3$ as

$$\mathbf{z}(\mathbf{r}_1)=\Pi(\mathbf{r}_1)(\mathcal{S}(\mathbf{e}_1)\mathbf{r}_1-\boldsymbol{\kappa}_{\mathcal{L}}d) \tag{9}$$

meaning that (8) can be rewritten as $\dot{\mathbf{r}}_1(t)=d^{-1}\|\mathbf{v}_{\mathcal{L}}(t)\|\mathcal{S}(\mathbf{z}(\mathbf{r}_1(t)))\mathbf{r}_1(t)$, i.e., the error $\mathbf{z}(\mathbf{r}_1)$ physically represents the nondimensional angular velocity of $\mathbf{r}_1$. The error is defined to be velocity-independent, depending on the characteristics of the leader's path and not on the velocity with which it is described. From its definition, it follows that if $\mathbf{z}(\mathbf{r}_1^\star)=\mathbf{0}$, then $\mathbf{r}_1^\star$ is an equilibrium point of (8).

Solving for the equilibrium point, two solutions emerge, depending exclusively on the parameters $\kappa_{\mathcal{L}}d$ and $\tau_{\mathcal{L}}d$ (or alternatively on $\boldsymbol{\kappa}_{\mathcal{L}}d$). They are $\mathbf{r}_1^\star,\bar{\mathbf{r}}_1^\star:\Omega_{\boldsymbol{\kappa}}\backslash\{(\tau_{\mathcal{L}},0,\kappa_{\mathcal{L}})\in\mathbb{R}^3:\kappa_{\mathcal{L}}>1\wedge\tau_{\mathcal{L}}=0\}\to\mathcal{S}^2$ defined as

$$\mathbf{r}_1^\star(\boldsymbol{\kappa}_{\mathcal{L}}d)=\begin{bmatrix}\mathrm{r}_{11}^\star(\boldsymbol{\kappa}_{\mathcal{L}}d)\\ \mathrm{r}_{12}^\star(\boldsymbol{\kappa}_{\mathcal{L}}d)\\ \mathrm{r}_{13}^\star(\boldsymbol{\kappa}_{\mathcal{L}}d)\end{bmatrix}=\begin{bmatrix}\sqrt{\frac{\tilde{\mathrm{r}}_{11}^2}{2}+\sqrt{(d\tau_{\mathcal{L}})^2+\left(\frac{\tilde{\mathrm{r}}_{11}^2}{2}\right)^2}}\\ -\dfrac{1-\mathrm{r}_{11}^{\star 2}(\boldsymbol{\kappa}_{\mathcal{L}}d)}{\kappa_{\mathcal{L}}d}\\ \dfrac{1-\mathrm{r}_{11}^{\star 2}(\boldsymbol{\kappa}_{\mathcal{L}}d)}{\mathrm{r}_{11}^\star(\boldsymbol{\kappa}_{\mathcal{L}}d)}\frac{\tau_{\mathcal{L}}}{\kappa_{\mathcal{L}}}\end{bmatrix} \tag{10}$$

and

$$\bar{\mathbf{r}}_1^\star(\boldsymbol{\kappa}_{\mathcal{L}}d)=\mathcal{R}_y(\pi)\mathbf{r}_1^\star(\boldsymbol{\kappa}_{\mathcal{L}}d) \tag{11}$$

where $\tilde{\mathrm{r}}_{11}^2:=1-d^2(\kappa_{\mathcal{L}}^2+\tau_{\mathcal{L}}^2)$ and $\mathcal{R}_y(\pi)$ is half of a full rotation around $\mathbf{e}_2$. We observe that $\mathrm{r}_{11}^\star(\cdot)$ and $\mathrm{r}_{12}^\star(\cdot)$, in (10), are continuous in their domain, while $\mathrm{r}_{13}^\star(\cdot)$ is discontinuous for $\kappa_{\mathcal{L}}d>1\wedge\tau_{\mathcal{L}}=0$. For $\kappa_{\mathcal{L}}d>1\wedge\tau_{\mathcal{L}}=0$, we extend (10) and (11) (by considering the limit $\tau_{\mathcal{L}}\to 0$) as

$$\mathbf{r}_1^\star(\boldsymbol{\kappa}_{\mathcal{L}}d),\bar{\mathbf{r}}_1^\star(\boldsymbol{\kappa}_{\mathcal{L}}d)=\begin{bmatrix}\mathrm{r}_{11}^\star(\boldsymbol{\kappa}_{\mathcal{L}}d)\\ \mathrm{r}_{12}^\star(\boldsymbol{\kappa}_{\mathcal{L}}d)\\ \mathrm{r}_{13}^\star(\boldsymbol{\kappa}_{\mathcal{L}}d)\end{bmatrix}=\begin{bmatrix}0\\ -\dfrac{1}{\kappa_{\mathcal{L}}d}\\ \pm\sqrt{1-\dfrac{1}{(\kappa_{\mathcal{L}}d)^2}}\end{bmatrix}. \tag{12}$$

When solving $\mathbf{z}(\mathbf{r}_1^\star)=\mathbf{0}$ for $\mathbf{r}_1^\star$, an additional relation is be found, namely $\boldsymbol{\kappa}_{\mathcal{L}}^T\mathbf{r}_1^\star(\boldsymbol{\kappa}_{\mathcal{L}}d)=(\tau_{\mathcal{L}}/\mathrm{r}_{11}^\star(\boldsymbol{\kappa}_{\mathcal{L}}d))$, which is important later in this article.

Corollary 1 suggests that $\mathbf{r}_1^\star(\boldsymbol{\kappa}_{\mathcal{L}}d)$ is stable, while $\bar{\mathbf{r}}_1^\star(\boldsymbol{\kappa}_{\mathcal{L}}d)$ is unstable. As expected, the stable solution corresponds to a trailer being pulled (see Fig. 2) and the unstable solution corresponds to a trailer being pushed.

Note also that $\mathbf{r}_1^\star(\mathbf{0})=\mathbf{r}_1^\star(\pm\infty\mathbf{e}_1)=\mathbf{e}_1$, which means that a leader describing a rectilinear path leads to the same leader–follower configuration, encoded by $\mathbf{r}_1^\star(\cdot)$, as a leader describing a helix with infinite torsion. In both cases, the leader is in front of the trailer, i.e., ${}^{\mathcal{L}}\mathbf{p}_{\mathcal{L}|\mathcal{T}}^\star=d\mathbf{e}_1$. This result should be expected as a helix with infinite torsion is a rectilinear path.

In Fig. 2, the leader describes a trimming path in solid black and the paths in dashed black are the follower's equilibrium paths for different combinations of $\kappa_{\mathcal{L}}d$. Fig. 2 shows the effect of the design parameter d, which effectively encodes how sensitive the followers are to the leader motion. In the limit case where $d\to 0$, the follower exactly mimics the leader;

[2]The restriction $\kappa_{\mathcal{L}}d<1$ can be lifted for trimming paths with $\tau_{\mathcal{L}}\neq 0$

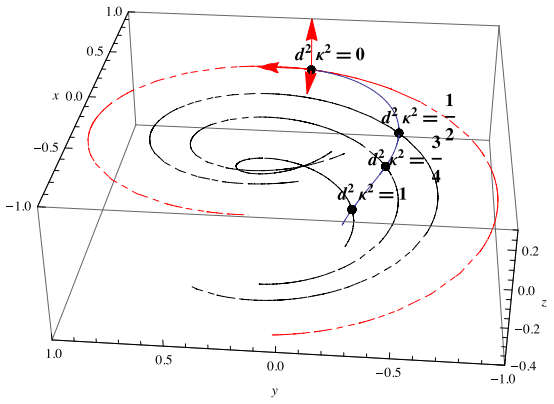

Fig. 2. Leader describing helix motion ($\kappa_{\mathcal{L}} = 1$, $\tau_{\mathcal{L}} = 0.1$) and trailer's hinge position (marked with ●) with respect to leader's reference frame $\{\mathcal{L}\}$ (${}^{\mathcal{I}}_{\mathcal{L}}\mathcal{R}$ is the oriented set of axes where the first axis ${}^{\mathcal{I}}_{\mathcal{L}}\mathcal{R}\mathbf{e}_1$ is tangent to the path).

on the other end of the spectrum, when $d \to \infty$, the follower is completely insensitive to what the leader does.[3] However, as discussed in Section III, if $t \mapsto \|\boldsymbol{\omega}_{\mathcal{F}}(t)\|$ is *too* large, which might occur for *small* d, the planned trajectory might be infeasible—depending on the follower's flight envelope. As such, there is a tradeoff between mimicking the leader and the feasibility of the planned trajectory.

There are two equilibrium solutions, $\mathbf{r}_1^\star(\cdot)$ and $\bar{\mathbf{r}}_1^\star(\cdot)$, identified in (10) and (11), respectively. Next, we prove that $\mathbf{r}_1^\star(\cdot)$ is (locally) exponentially stable, while $\bar{\mathbf{r}}_1^\star(\cdot)$ is unstable; afterward, we prove that $\mathbf{r}_1^\star(\cdot)$ is, in fact, AGAS.

Proposition 2: Consider a leader vehicle describing a trimming path and a trailer with kinematics (6). If $\tau_{\mathcal{L}} \neq 0$, then the equilibrium $\mathbf{r}_1^\star(\boldsymbol{\kappa}_{\mathcal{L}} d)$ is (locally) exponentially stable and the equilibrium $\bar{\mathbf{r}}_1^\star(\boldsymbol{\kappa}_{\mathcal{L}} d)$ is unstable.

Proof: Without loss of generality, assume $v_{\mathcal{L}}(t)d = 1$ for all $t \geq 0$ (see Remark 2). For a trimming path, $\dot{\boldsymbol{\kappa}}_{\mathcal{L}}(t) = \mathbf{0}$ for all $t \geq 0$, and system (8) is autonomous. In addition, it is possible to find an autonomous system of the form $\dddot{\mathrm{r}}_{11}(t) = f(\mathrm{r}_{11}(t), \dot{\mathrm{r}}_{11}(t), \ddot{\mathrm{r}}_{11}(t))$ when $\tau_{\mathcal{L}} \neq 0$ and with $f : \mathbb{R}^3 \to \mathbb{R}$. Denoting $\mathbf{x}(t) = [\mathrm{r}_{11}(t)\, \dot{\mathrm{r}}_{11}(t)\, \ddot{\mathrm{r}}_{11}(t)]^T$ and $\dot{\mathbf{x}}(t) = \mathbf{f}(\mathbf{x}(t))$, it follows that $\mathbf{x}^\star \in \{\begin{bmatrix}\mathrm{r}_{11}^\star & 0 & 0\end{bmatrix}^T, \begin{bmatrix}\bar{\mathrm{r}}_{11}^\star & 0 & 0\end{bmatrix}^T\}$ are the equilibria of the system. A linearization procedure around each of the equilibria yields $\frac{\partial \mathbf{f}(\mathbf{x})}{\partial \mathbf{x}}|_{\mathbf{x}=\mathbf{x}^\star}$, at shown on top of the next page, with $+\mathrm{r}_{11}^\star$ for $\mathbf{x}^\star = \begin{bmatrix}\mathrm{r}_{11}^\star & 0 & 0\end{bmatrix}$, and $-\mathrm{r}_{11}^\star$ for $\mathbf{x}^\star = \begin{bmatrix}\bar{\mathrm{r}}_{11}^\star & 0 & 0\end{bmatrix}$ (recall that $\mathrm{r}_{11}^\star = -\bar{\mathrm{r}}_{11}^\star$). With the help of the Hurwitz criterion, one infers the exponential stability of $\begin{bmatrix}\mathrm{r}_{11}^\star & 0 & 0\end{bmatrix}$ and the instability of $\begin{bmatrix}\bar{\mathrm{r}}_{11}^\star & 0 & 0\end{bmatrix}$ for the linearized system. Moreover, these conclusions extend to the nonlinear system $\dddot{\mathrm{r}}_{11}(t) = f(\mathrm{r}_{11}(t), \dot{\mathrm{r}}_{11}(t), \ddot{\mathrm{r}}_{11}(t))$. □

Remark 2: If $\inf_{t\geq 0} v_{\mathcal{L}}(t) > 0$, there exists an invertible mapping from time instant t to the leader path arc-length $\gamma_{\mathcal{L}}$, namely $\gamma_{\mathcal{L}} = f_{\mathcal{L}}(t) := \int_0^t (v_{\mathcal{L}}(\tau)/d)d\tau \Leftrightarrow t = f_{\mathcal{L}}^{-1}(\gamma_{\mathcal{L}})$. Then, given any function of time $\mathbf{f} : \mathbb{R}_{\geq 0} \to \mathbb{R}^3$, it follows that $(\partial \mathbf{f}(f_{\mathcal{L}}^{-1}(\gamma_{\mathcal{L}}))/\partial \gamma_L) = (\partial \mathbf{f}(t)/\partial t)|_{t=f_{\mathcal{L}}^{-1}(\gamma_L)} (\partial f_{\mathcal{L}}^{-1}(\gamma_L)/\partial \gamma_L) = (\partial \mathbf{f}(t)/\partial t)(1/v_{\mathcal{L}}(t)d^{-1})|_{t=f_{\mathcal{L}}^{-1}(\gamma_L)}$. For example, (8) becomes $(d\mathbf{r}_1/d\gamma_L) = \Pi(\mathbf{r}_1)\mathbf{e}_1 + \mathcal{S}(\mathbf{r}_1)\boldsymbol{\kappa}_{\mathcal{L}} d$ and (13) becomes $(dV/d\gamma_L) = -2\mathrm{r}_{11}V$. Moreover, note that $(d\mathbf{r}_1/d\gamma_L)$ is autonomous when the leader describes a trimming path.

We now present one of our main contributions that establishes the almost global asymptotic stability (AGAS) of $\mathbf{r}_1^\star(\boldsymbol{\kappa}_{\mathcal{L}} d)$ [and instability of $\bar{\mathbf{r}}_1^\star(\boldsymbol{\kappa}_{\mathcal{L}} d)$].

Theorem 1: Consider a leader vehicle describing a trimming path and a trailer with kinematics (6). If $\mathbf{r}_1(0) \in \mathcal{S}^2 \backslash \{\bar{\mathbf{r}}_1^\star\}$ and

1) $\kappa_{\mathcal{L}} = 0$ or
2) $0 < \kappa_{\mathcal{L}} d < 1$ or
3) $\kappa_{\mathcal{L}} d \geq 1$ and $\tau_{\mathcal{L}} \neq 0$

then the leader and follower vehicles converge to a rigid formation with a relative position vector given by ${}^{\mathcal{L}}\mathbf{p}_{\mathcal{L}|\mathcal{T}}^\star(\boldsymbol{\kappa}_{\mathcal{L}} d) = d\mathbf{r}_1^\star(\boldsymbol{\kappa}_{\mathcal{L}} d)$, corresponding to an AGAS equilibrium solution.

Proof: Consider the first scenario where $\kappa_{\mathcal{L}} = 0$, in which case $t \mapsto {}^{\mathcal{I}}_{\mathcal{L}}\mathcal{R}(t)$ is ill-defined. Then, Lemma 1 (take $\epsilon = 1$) guarantees that $t \mapsto \mathrm{r}_{11}(t)$ converges to 1 as long as $\mathrm{r}_{11}(0) \neq -1$. Equivalently, $t \mapsto \mathbf{r}_1(t)$ converges to $\mathbf{e}_1 = \mathbf{r}_1^\star(\mathbf{0})$. For the second scenario, where $0 < \kappa_{\mathcal{L}} d < 1$, $t \mapsto {}^{\mathcal{I}}_{\mathcal{L}}\mathcal{R}(t)$ is always well defined. Consider then the error defined in (9), the Lyapunov function $\tilde{V}(\mathbf{z}(\mathbf{r}_1)) = (1/2)\|\mathbf{z}(\mathbf{r}_1)\|^2$ and denote $t \mapsto V(t) = \tilde{V}(\mathbf{z}(\mathbf{r}_1(t)))$. Along a solution of (8), it follows that:

$$\dot{V}(t) = -2v_{\mathcal{L}}(t)d^{-1}\mathrm{r}_{11}(t)V(t). \tag{13}$$

Note that $t \mapsto V(t) = \tilde{V}(\mathbf{z}(\mathbf{r}_1(t)))$ is bounded by definition, since $\mathcal{S}^2 \ni \mathbf{r}_1 \mapsto \mathbf{z}(\mathbf{r}_1)$ is bounded. In addition, it follows from (13) that $V(t) = V(0)\exp(\int_0^t -2v_{\mathcal{L}}(\tau)d^{-1}\mathrm{r}_{11}(\tau)d\tau)$, where $V(0) = 0 \Leftrightarrow \mathbf{r}_1(0) = \mathbf{r}_1^\star(\boldsymbol{\kappa}_{\mathcal{L}} d) \vee \mathbf{r}_1(0) = \bar{\mathbf{r}}_1^\star(\boldsymbol{\kappa}_{\mathcal{L}} d)$. Assume $\mathbf{r}_1(t) \in \Omega_3(\epsilon) = \{\mathbf{x} \in \mathcal{S}^2 : \mathbf{x}^T\mathbf{e}_1 < -\epsilon\}\backslash\{\bar{\mathbf{r}}_1^\star\}$, for some $\epsilon \in (0, 1)$ and for all $t \geq 0$. In that case, it follows that $V(t) \geq V(0)\exp(2v_{\mathcal{L}}^{\min}d^{-1}\epsilon t)$, which is unbounded in time. Consequently, $\mathbf{r}_1(t)$ leaves the set $\Omega_3(\epsilon)$ for some $t > 0$, entering the set $\Omega_2(\epsilon)$. At that point, Lemma 1 guarantees $\mathrm{r}_{11}(t) > \epsilon$ for all $t \geq T > 0$ and for some T; when that happens, it follows from (13) that $t \mapsto V(t)$ converges exponentially fast to zero (because $\dot{V}(t) \leq -2v_{\mathcal{L}}^{\min}d^{-1}\epsilon V(t)$), while $t \mapsto \mathbf{r}_1(t)$ converges exponentially fast to $\mathbf{r}_1^\star(\boldsymbol{\kappa}_{\mathcal{L}} d)$.

Finally, consider the last case where $\tau_{\mathcal{L}} \neq 0$ and $\kappa_{\mathcal{L}} d \geq 1$. For brevity, denote $\bar{V} = \limsup_{t\to\infty} V(t)$, $\underline{V} = \liminf_{t\to\infty} V(t)$, and $\phi(t_2, t_1) = \exp(-\int_{t_1}^{t_2} v_{\mathcal{L}}(\tau)d^{-1}\mathrm{r}_{11}(\tau)d\tau)$. It follows from (13) that, if $V(t_1) > 0$ for some time instant, $t_1 \geq 0$, then $\phi(t_2, t_1) = ((V(t_2)/V(t_1)))^{1/2}$. Consider now also $\mathcal{S}^2 \ni \mathbf{r}_1 \mapsto \tilde{s}(\mathbf{r}_1) := (\tau_{\mathcal{L}}/|\tau_{\mathcal{L}}|)\boldsymbol{\kappa}_{\mathcal{L}}^T\mathbf{r}_1$, which is bounded ($|\tilde{s}(\cdot)| \leq \|\boldsymbol{\kappa}_{\mathcal{L}}\|$), and denote $t \mapsto s(t) = \tilde{s}(\mathbf{r}_1(t))$. Along a solution of (8), it follows that

$$\dot{s}(t) = -v_{\mathcal{L}}(t)d^{-1}(\mathrm{r}_{11}(t)s(t) - |\tau_{\mathcal{L}}|)$$

where $\dot{\boldsymbol{\kappa}}_{\mathcal{L}}(t) = \mathbf{0}$ has been used, since the theorem is restricted to the trimming paths. It then follows that $s(t) = \phi(t, 0)s(0) + |\tau_{\mathcal{L}}| \int_0^t \phi(s, 0)v_{\mathcal{L}}(s)d^{-1}ds$. Without loss of generality, and for the purpose of analysis, we may assume $s(0) = 0$. In addition, and again without loss of generality, assume that $v_{\mathcal{L}}(t)d^{-1} = 1$

[3] In fact, if the leader describes a path in a bounded space and $d \to \infty$, then the follower stays at rest all the time.

$$\frac{\partial \mathbf{f}(\mathbf{x})}{\partial \mathbf{x}}|_{\mathbf{x}=\mathbf{x}^\star} = \begin{bmatrix} 0 & 1 & 0 \\ 0 & 0 & 1 \\ -2\big(\pm \mathrm{r}_{11}^\star\big)\sqrt{(d\tau_{\mathcal{L}})^2 + \left(\frac{\tilde{\mathrm{r}}_{11}^2}{2}\right)^2} & -\big(6\mathrm{r}_{11}^{\star 2} - 1 + \|\boldsymbol{\kappa}_{\mathcal{L}} d\|^2\big) & -4\big(\pm \mathrm{r}_{11}^\star\big) \end{bmatrix}$$

for all $t \geq 0$ (see Remark 2). In that case, it follows that:

$$s(t) = |\tau_{\mathcal{L}}| \int_0^t \sqrt{\frac{V(s)}{V(0)}} ds. \tag{14}$$

It follows from (14) that $\bar{V} = 0$; otherwise, $\lim_{t\to\infty} s(t) = \infty$. Let us now analyze (14) assuming $\bar{V} \neq 0$, leading us to a contradiction whose ultimate implication is that in fact $\bar{V} = 0$. Suppose then that $\bar{V} \neq 0$, in which case $t \mapsto V(t)$ must asymptotically cross the interval $[\bar{V}, \bar{V}] = [0, \bar{V}]$ infinitely many times. Consider then the interval $[(1/4)\bar{V}, (1/2)\bar{V}] \subset [0, \bar{V}]$, and note that since $-2\, V(t) \leq \dot{V}(t) < 2\, V(t)$ [see (13)], then it takes, in the best case scenario, a time interval of $\Delta t = \ln(2) > 0$ for $t \mapsto V(t)$ to cross the interval $[(1/4)\bar{V}, (1/2)\bar{V}] \subset [0, \bar{V}]$. As such, consider two time instants t_2, t_1, such that $t_2 \geq t_1 + \ln(2) \geq \ln(2)$ and such that $V(t_1) = (1/2)\bar{V}$ and $V(t_2) = (1/4)\bar{V}$ (or alternatively, such that $V(t_1) = (1/4)\bar{V}$ and $V(t_2) = (1/2)\bar{V}$). Then, $\int_{t_1}^{t_2}((V(s)/V(0)))^{1/2} ds \geq \int_{t_1}^{t_1+\ln(2)}((\bar{V}/4V(0)))^{1/2} ds = ((\bar{V}/4V(0)))^{1/2}\ln(2) > 0$. Since $t \mapsto V(t)$ must asymptotically cross the interval $[\bar{V}, \bar{V}] = [0, \bar{V}]$ infinitely many times, it follows from the previous discussion that $\lim_{t\to\infty} \int_0^t ((V(s)/V(0)))^{1/2} ds = \infty$, and therefore, $\lim_{t\to\infty} s(t) = \infty$, which is not possible. This means that $\bar{V}$ is in fact 0, and therefore, $\lim_{t\to\infty} V(t) = 0$, since $\bar{V} = \bar{V} = 0$. Since $\lim_{t\to\infty} V(t) = 0$, it follows that $\lim_{t\to\infty} \mathbf{r}_1(t) = \mathbf{r}_1^\star(\boldsymbol{\kappa}_{\mathcal{L}} d)$ or $\lim_{t\to\infty} \mathbf{r}_1(t) = \bar{\mathbf{r}}_1^\star(\boldsymbol{\kappa}_{\mathcal{L}} d)$—the possibility of alternating infinitely fast between $\mathbf{r}_1^\star(\boldsymbol{\kappa}_{\mathcal{L}} d)$ and $\bar{\mathbf{r}}_1^\star(\boldsymbol{\kappa}_{\mathcal{L}} d)$ is excluded, since $t \mapsto \dot{\mathbf{r}}_1(t)$ is bounded. Now, recall (13) and note that if $\lim_{t\to\infty} \mathrm{r}_{11}(t) = \bar{\mathrm{r}}_{11}^\star(\boldsymbol{\kappa}_{\mathcal{L}} d) < 0$, then $\lim_{t\to\infty} V(t) = \infty$, which is impossible. Thus, it follows that $\lim_{t\to\infty} \mathbf{r}_1(t) = \mathbf{r}_1^\star(\boldsymbol{\kappa}_{\mathcal{L}} d)$, where $\mathrm{r}_{11}^\star(\boldsymbol{\kappa}_{\mathcal{L}} d) > 0$. □

Theorem 1 states that the equilibrium formation ${}^{\mathcal{L}}\mathbf{p}_{\mathcal{L}|\mathcal{T}}^\star(\boldsymbol{\kappa}_{\mathcal{L}} d) = d\mathbf{r}_1^\star(\boldsymbol{\kappa}_{\mathcal{L}} d)$ is AGAS while ${}^{\mathcal{L}}\mathbf{p}_{\mathcal{L}|\mathcal{T}}^\star(\boldsymbol{\kappa}_{\mathcal{L}} d) = d\bar{\mathbf{r}}_1^\star(\boldsymbol{\kappa}_{\mathcal{L}} d)$ is a second unstable equilibrium solution. Physically, these two equilibrium solutions correspond to a trailer being pulled ($\mathbf{e}_1^{T\,\mathcal{L}}\mathbf{p}_{\mathcal{L}|\mathcal{T}}^\star(\boldsymbol{\kappa}_{\mathcal{L}} d) = d\mathrm{r}_{11}^\star(\boldsymbol{\kappa}_{\mathcal{L}} d) > 0$) and a trailer being pushed ($\mathbf{e}_1^{T\,\mathcal{L}}\mathbf{p}_{\mathcal{L}|\mathcal{T}}^\star(\boldsymbol{\kappa}_{\mathcal{L}} d) = d\bar{\mathrm{r}}_{11}^\star(\boldsymbol{\kappa}_{\mathcal{L}} d) < 0$), respectively. Note that Theorem 1 guarantees almost global asymptotically stability of $\mathbf{r}_1^\star(\boldsymbol{\kappa}_{\mathcal{L}} d)$, while Proposition 2 guarantees the local exponential stability of $\mathbf{r}_1^\star(\boldsymbol{\kappa}_{\mathcal{L}} d)$.

Next, we discuss some of the properties of the equilibria $\mathbf{r}_1^\star(\cdot)$ and $\bar{\mathbf{r}}_1^\star(\cdot)$, when $\tau_{\mathcal{L}} = 0$ and $\kappa_{\mathcal{L}} d > 1$ and when $\tau_{\mathcal{L}} = 0$ and $\kappa_{\mathcal{L}} d = 1$.

Lemma 2: Consider a leader vehicle describing a trimming path, with $\tau_{\mathcal{L}} = 0$ and $\kappa_{\mathcal{L}} d > 1$, and a trailer with kinematics (6). Then, neither $\mathbf{r}_1^\star(\boldsymbol{\kappa}_{\mathcal{L}} d)$ nor $\bar{\mathbf{r}}_1^\star(\boldsymbol{\kappa}_{\mathcal{L}} d)$, as defined in (12), is asymptotically stable.

Proof: If $\tau_{\mathcal{L}} = 0$ and $\kappa_{\mathcal{L}} d > 1$, then $\mathbf{r}_1^\star(\boldsymbol{\kappa}_{\mathcal{L}} d), \bar{\mathbf{r}}_1^\star(\boldsymbol{\kappa}_{\mathcal{L}} d) = [0 \; -(\kappa_{\mathcal{L}} d)^{-1} \pm (1 - (\kappa_{\mathcal{L}} d)^{-2})^{1/2}]^T$. As such, $\mathrm{r}_{13}^\star, \bar{\mathrm{r}}_{13}^\star = \pm(1 - (\kappa_{\mathcal{L}} d)^{-2})^{1/2} \neq 0$, since $\kappa_{\mathcal{L}} d > 1$. When $\tau_{\mathcal{L}} = 0$, it follows from (8) that $\dot{\mathrm{r}}_{13}(t) = -v_{\mathcal{L}}(t) d^{-1} \mathrm{r}_{11}(t) \mathrm{r}_{13}(t)$. Now, recall (13), and assume that $\mathrm{r}_{13}(0) \neq 0$ and that $V(0) \neq 0 \Leftrightarrow \mathbf{r}_1(0) \neq \mathbf{r}_1^\star(\boldsymbol{\kappa}_{\mathcal{L}} d) \wedge \mathbf{r}_1(0) \neq \bar{\mathbf{r}}_1^\star(\boldsymbol{\kappa}_{\mathcal{L}} d)$. Now, assume that either $\mathbf{r}_1^\star(\boldsymbol{\kappa}_{\mathcal{L}} d)$ or $\bar{\mathbf{r}}_1^\star(\boldsymbol{\kappa}_{\mathcal{L}} d)$ is asymptotically stable, which implies that $\lim_{t\to\infty} V(t) = 0$. Since $\mathrm{r}_{13}(t) = \mathrm{r}_{13}(0)\exp(\int_0^t -v_{\mathcal{L}}(\tau) d^{-1} \mathrm{r}_{11}(\tau) d\tau)$ and, by assumption, $\lim_{t\to\infty} \mathrm{r}_{13}(t) = \pm(1 - (\kappa_{\mathcal{L}} d)^{-2})^{1/2}$, it follows that $\exp(\int_0^\infty -v_{\mathcal{L}}(\tau) d^{-1} \mathrm{r}_{11}(\tau) d\tau) = \pm(1 - (\kappa_{\mathcal{L}} d)^{-2})^{1/2} \mathrm{r}_{13}^{-1}(0)$. On the other hand, it follows from (13) that $V(t) = V(0)\exp(\int_0^t -2 v_{\mathcal{L}}(\tau) d^{-1} \mathrm{r}_{11}(\tau) d\tau)$, and therefore, $\lim_{t\to\infty} V(t) = (1 - (\kappa_{\mathcal{L}} d)^{-2}/\mathrm{r}_{13}^2(0)) V(0) \neq 0$. As such, a contradiction has been reached, implying that neither $\mathbf{r}_1^\star(\boldsymbol{\kappa}_{\mathcal{L}} d)$ nor $\bar{\mathbf{r}}_1^\star(\boldsymbol{\kappa}_{\mathcal{L}} d)$ is asymptotically stable. □

Lemma 3: Consider a leader vehicle describing a trimming path, with $\tau_{\mathcal{L}} = 0$ and $\kappa_{\mathcal{L}} d = 1$, and a trailer with kinematics (6). Then, the equilibrium point $\mathbf{r}_1^\star(\boldsymbol{\kappa}_{\mathcal{L}} d) = \bar{\mathbf{r}}_1^\star(\boldsymbol{\kappa}_{\mathcal{L}} d) = -\mathbf{e}_2$ is unstable.

Proof: First note that when $\tau_{\mathcal{L}} = 0$ and $\kappa_{\mathcal{L}} d = 1$, then (10) and (11) are in fact the same equilibrium point, to be specific, $\mathbf{r}_1^\star(\boldsymbol{\kappa}_{\mathcal{L}} d) = \bar{\mathbf{r}}_1^\star(\boldsymbol{\kappa}_{\mathcal{L}} d) = -\mathbf{e}_2$. For $\tau_{\mathcal{L}} = 0$, $\dot{\mathrm{r}}_{13}(t) = -v_{\mathcal{L}}(t) d^{-1} \mathrm{r}_{11}(t) \mathrm{r}_{13}(t)$, which follows from (8). If $\mathrm{r}_{13}(0) = 0$, it follows from the latter that $\mathrm{r}_{13}(t) = 0$ for all $t \geq 0$. With this in mind and assuming $\mathrm{r}_{13}(0) = 0$, we may parameterize $t \mapsto \mathbf{r}_1(t)$ as $\mathbf{r}_1(t) = [\sin(\psi(t)) \; -\cos(\psi(t)) \; 0]$, in which case the equilibrium $\mathbf{r}_1^\star(\boldsymbol{\kappa}_{\mathcal{L}} d) = \bar{\mathbf{r}}_1^\star(\boldsymbol{\kappa}_{\mathcal{L}} d) = -\mathbf{e}_2$ is parameterized as $\psi^\star = 0$. For this choice, and since $\tau_{\mathcal{L}} = 0$ and $\kappa_{\mathcal{L}} d = 1$, it follows from (8) that $\dot{\psi}(t) = -v_{\mathcal{L}}(t) d^{-1}(1 - \cos(\psi(t)))$. For this system, $\psi^\star = 0$ is unstable. Indeed, suppose $\psi(0) \in [-(\pi/2), 0)$; then, $\dot{\psi}(t) \leq -v_{\mathcal{L}}^{\min} d^{-1}(1 - \cos(\psi(0))) < 0$ for as long as $\psi(t) \in [-(\pi/2), -\psi(0))$; this in turn implies that $t \mapsto \psi(t)$ does not remain arbitrarily close to $\psi^\star = 0$, regardless of how close $\psi(0)$ is of $\psi^\star = 0$, which means $\psi^\star = 0$, and therefore, $\mathbf{r}_1^\star(\boldsymbol{\kappa}_{\mathcal{L}} d) = \bar{\mathbf{r}}_1^\star(\boldsymbol{\kappa}_{\mathcal{L}} d) = -\mathbf{e}_2$ is unstable. □

Note that Lemma 3 establishes the instability of $\mathbf{r}_1^\star(\boldsymbol{\kappa}_{\mathcal{L}} d) = \bar{\mathbf{r}}_1^\star(\boldsymbol{\kappa}_{\mathcal{L}} d) = -\mathbf{e}_2$, but, at least, a lack of asymptotic stability of the equilibrium should be expected. Indeed, since there is only one equilibrium and given that $t \mapsto \mathbf{r}_1(t)$ lives in a closed set (with continuous dynamics), we should not expect the double equilibrium point to be asymptotically stable.

Remark 3: The time derivative (13) around the equilibrium $\mathbf{r}_1^\star(\boldsymbol{\kappa}_{\mathcal{L}} d)$ may be written as

$$\dot{V} = -v_{\mathcal{L}} d^{-1} \mathrm{r}_{11}^\star \left\| \frac{\partial \mathbf{z}}{\partial \mathbf{r}_1}|_{\mathbf{r}_1=\mathbf{r}_1^\star} \big(\mathbf{r}_1 - \mathbf{r}_1^\star\big) \right\|^2 + \mathcal{O}\big(\|\mathbf{r}_1 - \mathbf{r}_1^\star\|^2\big)$$

where it was assumed that $(\|\mathbf{v}_{\mathcal{L}}\|/d)$ is constant. This expression indicates that the convergence to the equilibrium is slower for smaller but positive $\mathrm{r}_{11}^\star(\boldsymbol{\kappa}_{\mathcal{L}} d)$, which occurs when $\tau_{\mathcal{L}}$ is *small* and $\kappa_{\mathcal{L}} d$ is *large* (i.e., $\tau_{\mathcal{L}} \approx 0$ and $\kappa_{\mathcal{L}} d \geq 1$). This

relates to Lemma 2, under which the equilibria lack asymptotic stability.

C. Leader Describing Nontrimming Paths

Theorem 1 guarantees that the final leader–follower formation is independent of the initialization of the planner—as long as $\mathbf{r}_1(0) \neq \bar{\mathbf{r}}_1^\star(\kappa_\mathcal{L} d)$—but it only applies for a leader describing a trimming path, which excludes a broad set of paths. For a leader describing a nontrimming path, one would also like to guarantee the same behavior, i.e., that the planned trajectory does not depend on the planner's initialization. The question that then arises is whether a unique attracting trajectory for the follower exists, which depends solely on the leader's path intrinsic properties, namely path curvature $\kappa_\mathcal{L}$ and path torsion $\tau_\mathcal{L}$, and the distance d.

For this purpose, consider then two solutions $t \mapsto \mathbf{r}_1^a(t)$ and $t \mapsto \mathbf{r}_1^b(t)$ of (8) with different initial conditions. If $t \mapsto \mathbf{r}_1^a(t)$ and $t \mapsto \mathbf{r}_1^b(t)$ converge to one another, regardless of different initial conditions, it logically follows that a unique equilibrium trajectory exists. This concept of an attracting trajectory is also studied in contraction analysis: "if all neighboring trajectories converge to each other (contraction behavior), global exponential convergence to a single trajectory can then be concluded" [31].

Theorem 2: Consider a leader whose curvature is bounded and satisfies $(\kappa_\mathcal{L}(t)d)^2 \leq (\kappa_\mathcal{L}^{\max} d)^2 < 1$ for all $t \geq 0$ and a trailer with kinematics (6). If $\mathbf{r}_1(0) \in \mathbf{\Omega}_1(0)$, then the final planned trajectory, encoded by $t \mapsto \mathbf{r}_1(t)$, does not depend on the initialization $\mathbf{r}_1(0)$, i.e., there is a unique attracting solution.

Proof: Consider two solutions $t \mapsto \mathbf{r}_1^a(t)$ and $t \mapsto \mathbf{r}_1^b(t)$ of (8) with different initial conditions, but where $\mathbf{r}_1^a(0), \mathbf{r}_1^b(0) \in \mathbf{\Omega}_1(0)$. In addition, consider the Lyapunov function $V(t) = 1 - \mathbf{r}_1^{aT}(t)\mathbf{r}_1^b(t)$, whose time derivative yields

$$\dot{V}(t) = -\upsilon_\mathcal{L}(t) d^{-1} \left(\mathbf{e}_1^T \mathbf{r}_1^a(t) + \mathbf{e}_1^T \mathbf{r}_1^b(t)\right) V(t).$$

Given the conditions of the theorem, Lemma 1 applies and, as a consequence, it follows that $t \mapsto \mathbf{r}_1^a(t)$ and $t \mapsto \mathbf{r}_1^b(t)$ enter the set $\mathbf{\Omega}_1((1 - (\kappa_\mathcal{L}^{\max} d)^2)^{1/2})$ in finite time and never leave that set afterward. Thus, after a finite time, $\dot{V}(t) \leq -\upsilon_\mathcal{L}(t) d^{-1} 2(1 - (\kappa_\mathcal{L}^{\max} d)^2)^{1/2} V(t)$, which implies that $t \mapsto V(t)$ converges exponentially fast to 0. Moreover, this implies that $t \mapsto \mathbf{r}_1^a(t)$ and $t \mapsto \mathbf{r}_1^b(t)$ converge exponentially fast to one another. Since $t \mapsto \mathbf{r}_1^a(t)$ and $t \mapsto \mathbf{r}_1^b(t)$ are the arbitrary trajectories of (8), it follows that there exists a unique attracting solution that all the solutions of (8) converge to. □

Remark 4: The results in Theorem 2 are valid as long as $t \mapsto {}^\mathcal{I}_\mathcal{L}\mathcal{R}(t)\mathbf{e}_1$ (i.e., the leader velocity direction) is well defined and continuously differentiable, regardless of whether or not the complete rotation matrix $t \mapsto {}^\mathcal{I}_\mathcal{L}\mathcal{R}(t)$ is ill-defined. In fact, we may write the Lyapunov function in Theorem 2 and its derivative as $V(t) = 1 - ({}^\mathcal{I}_\mathcal{T}\mathcal{R}^a(t)\mathbf{e}_1)^T ({}^\mathcal{I}_\mathcal{T}\mathcal{R}^b(t)\mathbf{e}_1)$ and $\dot{V}(t) = -\upsilon_\mathcal{L}(t) d^{-1} (({}^\mathcal{I}_\mathcal{L}\mathcal{R}(t)\mathbf{e}_1)^T ({}^\mathcal{I}_\mathcal{T}\mathcal{R}^a(t)\mathbf{e}_1) + ({}^\mathcal{I}_\mathcal{L}\mathcal{R}(t)\mathbf{e}_1)^T ({}^\mathcal{I}_\mathcal{T}\mathcal{R}^b(t)\mathbf{e}_1)) V(t)$, where $t \mapsto {}^\mathcal{I}_\mathcal{T}\mathcal{R}^i(t)$ for $i = \{a, b\}$ represents two different trailer rotation matrices, which evolve according to kinematics (6).

Theorem 2 loosely states that a nontrimming equilibrium solution exists and that all solutions, properly initialized, converge exponentially fast to that equilibrium. In other words, if a trailer starts behind the leader (a hemisphere of possible initial conditions), it converges to a moving point that lives in that same hemisphere. Note that the idea of an attracting solution is already present in Theorem 1, where $\mathbf{r}_1^\star(\kappa_\mathcal{L} d)$ is an AGAS solution. In Fig. 3(a), a leader describes a lemniscate path (a nontrimming path) and, for different initial conditions satisfying the conditions of Theorem 2, all trajectories converge to one another.

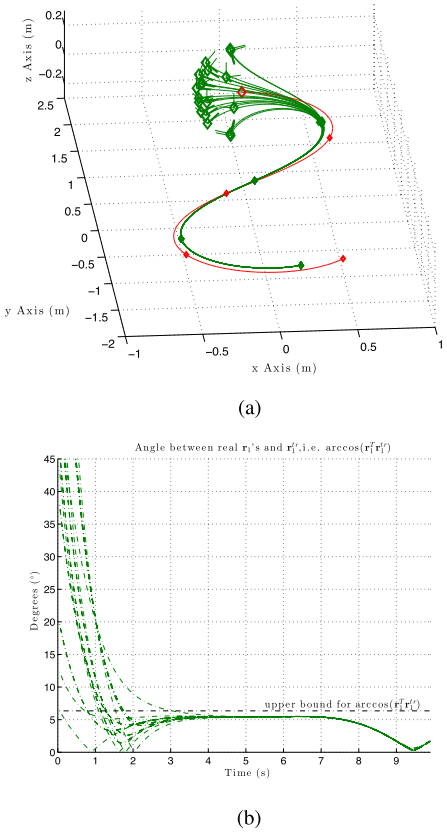

(a)

(b)

Fig. 3. Trailer trajectories for a leader describing a lemniscate path and for different initializations. (a) Leader in red and trailer in green with positions sampled four times (◇ for initial positions). (b) Angular distance between solutions $\mathbf{r}_1$ in Fig. 3(a) and solution $\mathbf{r}_1^\star$, in black upper bound from Theorem 3.

Theorem 2 applies to both trimming and nontrimming paths but, unlike Theorem 1, it does not provide any insight into the analytical solution of the attracting trajectory. However, intuition suggests that if $t \mapsto \boldsymbol{\kappa}_\mathcal{L}(t)$ varies slowly (with respect to the leader path arc-length), then we should expect $t \mapsto \mathbf{r}_1(t)$ to be *close* to $t \mapsto \mathbf{r}_1^\star(\boldsymbol{\kappa}_\mathcal{L}(t)d)$.[4] Fig. 3(b) shows the angular distance between the solutions shown in Fig. 3(a)—i.e., different solutions $t \mapsto \mathbf{r}_1(t)$ of (8)—and $t \mapsto \mathbf{r}_1^\star(\boldsymbol{\kappa}_\mathcal{L}(t)d)$. It is clear that all the angular distances converge to the same function, as predicted by Theorem 2. In the next theorem, we provide a bound for the angular distance that vanishes for the case when $\dot{\boldsymbol{\kappa}}_\mathcal{L}(t) = 0$ for all $t \geq 0$, as expected

[4]Note that $t \mapsto \mathbf{r}_1^\star(\boldsymbol{\kappa}_\mathcal{L}(t)d)$ is not a constant, because $t \mapsto \boldsymbol{\kappa}_\mathcal{L}(t)$ varies with time; rather, it is the equilibrium that would be obtained at each point of the leader path if this were a trimming path with curvature and torsion associated with that point of the path.

from Theorem 1. We emphasize that the bound does not depend explicitly on how $\boldsymbol{\kappa}_{\mathcal{L}}(\cdot)$ varies with time but rather on how it varies with the arc-length of the path. With that in mind, let the rate of change of the leader path curvature with respect to the leader path parameterization be defined as $\boldsymbol{\kappa}'_{\mathcal{L}}(t) \equiv \left[\tau'_{\mathcal{L}}(t)\ 0\ \kappa'_{\mathcal{L}}(t)\right]^T := (\dot{\boldsymbol{\kappa}}_{\mathcal{L}}(t)/v_{\mathcal{L}}(t))$.

Theorem 3: Consider a leader vehicle describing a nontrimming path with curvature satisfying $(\kappa_{\mathcal{L}}(t)d)^2 \leq (\kappa_{\mathcal{L}}^{\max}d)^2 < 1$ and $\|\boldsymbol{\kappa}'_{\mathcal{L}}(t)\| \leq \|\boldsymbol{\kappa}'_{\mathcal{L}}\|^{\max}$ for all $t \geq 0$. In addition, consider a trailer attached to the leader, with kinematics (6) and initialized such that $\mathbf{r}_1(0) \in \Omega_1(0)$. Under those conditions

$$\left[\frac{1-C^2}{1+C^2}, 1\right] \tag{15}$$

defines an invariant set and an ultimate bound on $t \mapsto \mathbf{r}_1^{\star T}(\boldsymbol{\kappa}_{\mathcal{L}}(t)d)\mathbf{r}_1(t)$, where

$$C > \frac{1}{2}\frac{\|\boldsymbol{\kappa}'_{\mathcal{L}}\|^{\max}d^2}{\sqrt{1-\kappa_{\mathcal{L}}^{\max}d}}\sup_{s\geq 0}\left\|\frac{d\mathbf{r}_1^{\star}(\boldsymbol{\gamma}_{\boldsymbol{\kappa}})}{d\boldsymbol{\gamma}_{\boldsymbol{\kappa}}}|_{\boldsymbol{\gamma}_{\boldsymbol{\kappa}}=\boldsymbol{\kappa}_{\mathcal{L}}(s)d}\right\|$$

with $\mathbf{r}_1^{\star}(\cdot)$ as defined in (10).

Proof: Consider the Lyapunov function

$$V(t) = 1 - \mathbf{r}_1^{\star T}(\boldsymbol{\kappa}_{\mathcal{L}}(t)d)\mathbf{r}_1(t) \equiv 1 - \cos(\theta(t))$$

where $\theta(t)$ is the angular distance between $\mathbf{r}_1^{\star}(t)$ and $\mathbf{r}_1(\boldsymbol{\kappa}_{\mathcal{L}}(t)d)$ [see Fig. 8(b)]. In addition, consider $t \mapsto \mathbf{r}_1^{\star}(\boldsymbol{\kappa}_{\mathcal{L}}(t)d)$, which varies according to the kinematics

$$\begin{aligned}\dot{\mathbf{r}}_1^{\star}(\boldsymbol{\kappa}_{\mathcal{L}}(t)d) = &-v_{\mathcal{L}}(t)\mathcal{S}\left(\mathbf{r}_1^{\star}(\boldsymbol{\kappa}_{\mathcal{L}}(t)d)\right)\mathbf{z}\left(\mathbf{r}_1^{\star}(\boldsymbol{\kappa}_{\mathcal{L}}(t)d)\right)\\ &+\ v_{\mathcal{L}}(t)\frac{d\mathbf{r}_1^{\star}(\boldsymbol{\gamma}_{\boldsymbol{\kappa}})}{d\boldsymbol{\gamma}_{\boldsymbol{\kappa}}}|_{\boldsymbol{\gamma}_{\boldsymbol{\kappa}}=\boldsymbol{\kappa}_{\mathcal{L}}(t)d}\boldsymbol{\kappa}'_{\mathcal{L}}(t)d\end{aligned} \tag{16}$$

where, by definition, $\mathbf{z}(\mathbf{r}_1^{\star}(\boldsymbol{\kappa}_{\mathcal{L}}(t)d)) = \mathbf{0}$ (for all t) and where $t \mapsto \boldsymbol{\kappa}'_{\mathcal{L}}(t)$ is the rate of change of curvature and torsion with respect to the leader's path arc-length. From (16), Lyapunov's time derivative yields

$$\begin{aligned}&\dot{V}(t)\\ &< -v_{\mathcal{L}}(t)d^{-1}\left(\mathbf{e}_1^T\mathbf{r}_1^{\star}(\boldsymbol{\kappa}_{\mathcal{L}}(t)d) + \mathbf{e}_1^T\mathbf{r}_1(t)\right)(V(t) - |\sin(\theta(t))|C)\\ &= -v_{\mathcal{L}}(t)d^{-1}\left(\mathbf{e}_1^T\mathbf{r}_1^{\star}(\boldsymbol{\kappa}_{\mathcal{L}}(t)d) + \mathbf{e}_1^T\mathbf{r}_1(t)\right)\\ &\quad\times(V(t) - \sqrt{V(t)(2-V(t))}C).\end{aligned}$$

Under the conditions of the theorem, Lemma 1 may be invoked to conclude that $t \mapsto \mathbf{r}_1(t)$ enters the set $\Omega_1((1-(\kappa_{\mathcal{L}}^{\max}d)^2)^{1/2})$ in finite time, and never leaves that set afterward. Moreover, under the conditions of the theorem, it follows that $\inf_{t\geq 0}\mathbf{e}_1^T\mathbf{r}_1^{\star}(\boldsymbol{\kappa}_{\mathcal{L}}(t)d) > 0$. It follows then that $t \mapsto \dot{V}(t)$ is negative if $V(t) - (V(t)(2-V(t)))^{1/2}C \geq 0 \Leftrightarrow V(t) \leq (2\ C^2/1+C^2)$, which is equivalent to

$$\cos(\theta(t)) \equiv \mathbf{r}_1^{\star T}(\boldsymbol{\kappa}_{\mathcal{L}}(t)d)\mathbf{r}_1(t) \leq \frac{1-C^2}{1+C^2}$$

and consequently $[(1-C^2/1+C^2), 1]$ is an ultimate bound and invariant set on $t \mapsto \mathbf{r}_1^{\star T}(\boldsymbol{\kappa}_{\mathcal{L}}(t)d)\mathbf{r}_1(t)$. □

Loosely speaking, Theorem 3 states that as a nontrimming path gets closer to a trimming path, i.e., as $\sup_{t\geq 0}\|\boldsymbol{\kappa}'_{\mathcal{L}}(t)\|$ becomes smaller, the attracting nontrimming solution $t \mapsto \mathbf{r}_1(t)$ gets closer to $t \mapsto \mathbf{r}_1^{\star}(\boldsymbol{\kappa}_{\mathcal{L}}(t)d)$.

Theorem 3 provides a bound on the angular distance between $t \mapsto \mathbf{r}_1(t)$ and $t \mapsto \mathbf{r}_1^{\star}(\boldsymbol{\kappa}_{\mathcal{L}}(t)d)$. In Fig. 3(b), the bound (15) is presented in dashed black. Note that all angular errors converge to one another and additionally the bound provides a measure of closeness of the attracting nontrimming solution to the trimming solution defined as in (10).

Remark 5: For the same reasons as in Remark 4, Theorem 3 is valid even when $t \mapsto {}^{\mathcal{I}}_{\mathcal{L}}\mathcal{R}(t)$ is ill-defined, i.e., even when the leader reference frame is ill-defined, the attracting solution still exists and is unique.

Theorem 4: Consider a leader vehicle describing a nontrimming path and a trailer with kinematics (6). In addition, assume that the velocity measurements $t \mapsto \mathbf{v}_{\mathcal{L}}^c(t)$ available to the follower are corrupted by measurement noise $t \mapsto \boldsymbol{\delta}_{\mathbf{v}_{\mathcal{L}}}(t)\|\mathbf{v}_{\mathcal{L}}(t)\|$, such that $\mathbf{v}_{\mathcal{L}}^c(t) = \mathbf{v}_{\mathcal{L}}(t) + \boldsymbol{\delta}_{\mathbf{v}_{\mathcal{L}}}(t)\|\mathbf{v}_{\mathcal{L}}(t)\|$. Under the presence of that noise, $t \mapsto \kappa_{\mathcal{L}}^c(t)$ denotes the corrupted leader path curvature and $t \mapsto \mathbf{r}_1^c(t)$ encodes the corrupted planned trajectory. If $(\kappa_{\mathcal{L}}(t)d)^2 \leq (\kappa_{\mathcal{L}}^{\max}d)^2 < 1$ and $(\kappa_{\mathcal{L}}^c(t)d)^2 \leq (\kappa_{\mathcal{L}}^{\max}d)^2 < 1$ for all $t \geq 0$ and $\mathbf{r}_1^c(0) \in \Omega_1(0)$, then $[(1-C^2/1+C^2), 1]$ where $C > (1/2)(1/(1-\kappa_{\mathcal{L}}^{\max}d)^{1/2})\sup_{t\geq 0}\|\boldsymbol{\delta}_{\mathbf{v}_{\mathcal{L}}}(t)\|$ defines an ultimate bound and an invariant set for $t \mapsto \mathbf{r}_1^c(t)^T\mathbf{r}_1(t)$, where $t \mapsto \mathbf{r}_1(t)$ is the attracting solution of (8).

The proof of Theorem 4 follows very closely that of Theorem 3, and for that reason, it is omitted for brevity. Theorem 4 implies that n followers can perform their planning independently (each vehicle having a different noise associated with the leader velocity measurement) and all solutions remain close to the attracting solution that would be obtained without noise. This provides the planning with robustness properties that other planning strategies do not have, especially those that focus on intervehicle distances (in [24] and [25]), where different initial conditions and disturbances have long-lasting effects on the planning.

Remark 6: Theorem 1 is partially recovered from Theorem 3, if the condition $\boldsymbol{\kappa}'_{\mathcal{L}}(t) = 0$ for all $t \geq 0$ is imposed. For that case, $\lim_{t\to\infty}\mathbf{r}_1^{\star T}(\boldsymbol{\kappa}_{\mathcal{L}}(t)d)\mathbf{r}_1(t) = 1$. Theorem 1 is not fully recovered, because Theorem 3 has a narrower set of allowed initial conditions and additionally Theorem 3 requires $\kappa_{\mathcal{L}}^{\max}d < 1$.

Remark 7: For all previously stated theorems, we have restricted the leader to possess a continuous direction of motion, i.e., $t \mapsto {}^{\mathcal{I}}_{\mathcal{L}}\mathcal{R}(t)\mathbf{e}_1$ to be always well defined. When such condition is not satisfied, a reinitialization of the planner occurs, i.e., $t \mapsto \mathbf{r}_1(t) = {}^{\mathcal{L}}_{\mathcal{I}}\mathcal{R}(t)\mathbf{e}_1$ suffers a discontinuity, and all theorems can be applied once again from the time instant at which the discontinuity occurs onward, disregarding all the past evolution of $t \mapsto \mathbf{r}_1(t)$.

D. Properties of the Followers' Path

As mentioned before, the trailer reference frame is a parallel transport reference frame. Following [30], it is possible to compute the trailer's path curvature $\kappa_{\mathcal{T}} : \mathbb{R}_{\geq 0} \to \mathbb{R}$ and torsion $\tau_{\mathcal{T}} : \mathbb{R}_{\geq 0} \to \mathbb{R}$, namely

$$\kappa_{\mathcal{T}}(t) = \frac{\sqrt{1-\mathrm{r}_{11}^2(t)}}{d|\mathrm{r}_{11}(t)|} \quad \text{and} \quad \tau_{\mathcal{T}}(t) = \frac{\kappa_{\mathcal{L}}\mathrm{r}_{13}(t)}{\mathrm{r}_{11}(t)(1-\mathrm{r}_{11}^2(t))}$$

where these are valid for time-varying $t \mapsto \boldsymbol{\kappa}_{\mathcal{L}}(t)$ (the solutions above are always well defined under the conditions

of Corollary 1). Consequently, they are also valid for a leader describing a trimming path, where $t \mapsto \boldsymbol{\kappa}_{\mathcal{L}}(t)$ is constant and $t \mapsto \mathbf{r}_1(t)$ converges to $\mathbf{r}_1^\star(\boldsymbol{\kappa}_{\mathcal{L}} d)$. In that case, it follows that $t \mapsto \kappa_{\mathcal{T}}(t)$ and $t \mapsto \tau_{\mathcal{T}}(t)$ also converge to constant values, namely $\kappa_{\mathcal{T}}^\star = ((1 - \mathrm{r}_{11}^{\star 2}(\boldsymbol{\kappa}_{\mathcal{L}} d))^{1/2}/d\mathrm{r}_{11}^\star(\boldsymbol{\kappa}_{\mathcal{L}} d))$ and $\tau_{\mathcal{T}}^\star = (\tau_{\mathcal{L}}/\mathrm{r}_{11}^{\star 2}(\boldsymbol{\kappa}_{\mathcal{L}} d))$. Therefore, for a leader describing a trimming path, the trailer also asymptotically describes a trimming path.

VIII. Convergence of the Trailer Reference Frame

In Section VII, we proved that the trailer hinge point $t \mapsto \mathbf{p}_{\mathcal{T}}(t)$ and the first axis $t \mapsto {}^{\mathcal{T}}_{\mathcal{T}}\mathcal{R}(t)\mathbf{e}_1$ converge to an equilibrium solution. However, for a nonlongitudinal $\bar{\mathbf{d}}$, the convergence of the complete rotation matrix $t \mapsto {}^{\mathcal{T}}_{\mathcal{T}}\mathcal{R}(t)$ to one solution is also required. The longitudinal direction $t \mapsto {}^{\mathcal{T}}_{\mathcal{T}}\mathcal{R}(t)\mathbf{e}_1$ converges according to the selection of the pitch and the yaw rates, as analyzed in Section VII. On the other hand, the convergence of the orthogonal space to $t \mapsto {}^{\mathcal{T}}_{\mathcal{T}}\mathcal{R}(t)\mathbf{e}_1$ depends on the choice of the roll rate, i.e., on $t \mapsto p_{\mathcal{T}}(t)$. This section is dedicated to the roll rate design and the properties that follow from its choice.

A. Roll Rate Design

Before conducting a discussion on the roll rate design, consider a leader and a follower living in a 1-D space. Then, the leader-following goal can be restated as $\mathrm{p}_{\mathcal{L}} - \mathrm{p}_{\mathcal{F}} = rd$ (with $r \in \{-1, 1\}$) from which two possible solutions arise and one must be chosen: either the leader is at the front at all times or at the back. In a 2-D environment, a similar ambiguity arises and, with a proper choice of yaw rate, one of the equilibrium points is rendered stable (pulled trailer) and the other is rendered unstable (pushed trailer).[5]

In [14], the 2-D case for $t \mapsto {}^{\mathcal{T}}_{\mathcal{T}}\mathcal{R}(t) \in \mathcal{SO}(2)$ was studied, so only one planned path came as a result from planning. However, the group of 2×2 orthogonal matrices, $\mathcal{R}^{2D} \in \mathcal{O}(2)$, is not connected. It can be seen as the union of two connected groups, with matrices that satisfy $\det(\mathcal{R}_1^{2D}) = 1$ and $\det(\mathcal{R}_2^{2D}) = -1$ (note the similarity with the 1-D term r).

However, in a 3-D setting, a rotation matrix $\mathcal{R}^{3D}$ corresponding to a rotation around, for example, the z-axis, can be of the form $\mathcal{R}_1^{3D} = \mathrm{diag}(\mathcal{R}_1^{2D}, 1)$ or $\mathcal{R}_2^{3D} = \mathrm{diag}(\mathcal{R}_2^{2D}, -1)$. This explains why an extra ambiguity, which does not exist in the 2-D case, arises when one moves to a 3-D space. Fig. 4 shows the two solutions $\mathcal{R}_1^{3D} \equiv \mathcal{R}_1^\star$ and $\mathcal{R}_2^{3D} \equiv \mathcal{R}_2^\star$.

To sum up, from 1-D to 2-D, one ambiguity arises, while from 2-D to 3-D, another ambiguity arises. As such, ${}^{\mathcal{T}}_{\mathcal{T}}\mathcal{R}$ has four equilibrium solutions, two solutions corresponding to a stable ${}^{\mathcal{T}}_{\mathcal{T}}\mathcal{R}\mathbf{e}_1$ (this analysis has been conducted in Section VII) and the other two corresponding to an unstable ${}^{\mathcal{T}}_{\mathcal{T}}\mathcal{R}\mathbf{e}_1$. We focus attention on the two solutions, where ${}^{\mathcal{T}}_{\mathcal{T}}\mathcal{R}\mathbf{e}_1$ is stable, with the objective of designing a roll rate that provides stability to one and instability to the other.

Definition 3: Consider a unit vector $\mathbf{n} \in \mathcal{S}^2$, which is chosen as the *preferred vertical direction* and a vehicle with the reference frame $(\mathcal{R}, \mathbf{p})$, where the rotation matrix rotates with angular velocity $\boldsymbol{\omega}$. Then, the vehicle is said to move in a *clockwise* direction if $\mathbf{n}^T\mathcal{R}\boldsymbol{\omega} > 0$, an *anticlockwise* direction if $\mathbf{n}^T\mathcal{R}\boldsymbol{\omega} < 0$, and an *indefinite* direction if $\mathbf{n}^T\mathcal{R}\boldsymbol{\omega} = 0$. In addition, the vehicle is said to *stand up* if $\mathbf{n}^T\mathcal{R}\mathbf{e}_3 > 0$, to *stand down* if $\mathbf{n}^T\mathcal{R}\mathbf{e}_3 < 0$, and to *stand indefinite* if $\mathbf{n}^T\mathcal{R}\mathbf{e}_3 = 0$.

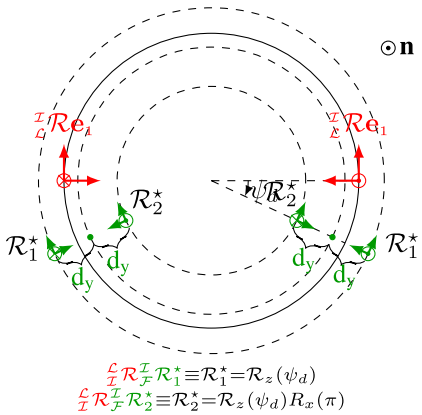

Fig. 4. Possible ${}^{\mathcal{L}}_{\mathcal{T}}\mathcal{R}$ configurations for a trailer point with longitudinal axis d and $\bar{\mathbf{d}} = \mathrm{d_y}\mathbf{e}_2$ ($\mathrm{d_y} > 0$).

Remark 8: The preferred vertical direction $\mathbf{n}$ is a parameter to be specified by the designer. For example, if a mission objective is to map a vertical wall, the preferred vertical should be selected as the normal to that wall.

Remark 9: In a 2-D setting, a trailer is either always standing up [this corresponds to $\det(\mathcal{R}^{2D}) = 1$] or always standing down [$\det(\mathcal{R}^{2D}) = -1$]. However, in a 3-D setting, a trailer can leave the plane and approach either of the 2-D solutions.

Consider a leader describing a clockwise circular path and an anticlockwise circular path, as shown in Fig. 4. The planning problem lies on deciding which path should be stable: the one corresponding to $\mathcal{R}_1^\star$ or the one corresponding to $\mathcal{R}_2^\star$. We decide on this problem by imposing the stable solution to be that where the trailer stands up (see Remark 9). Thus, a switch between $\mathcal{R}_1^\star$ and $\mathcal{R}_2^\star$ is required if the leader path changes from the clockwise to the anticlockwise direction (see Fig. 4). This behavior is proposed, because the leader's second axis ${}^{\mathcal{T}}_{\mathcal{L}}\mathcal{R}\mathbf{e}_2$ (and also the third axis ${}^{\mathcal{T}}_{\mathcal{L}}\mathcal{R}\mathbf{e}_3$) inverts its direction when moving from clockwise to anticlockwise paths and the planning should not be sensitive to such discontinuities.

A leader vehicle describing a planar path verifies $t \mapsto \mathbf{v}_{\mathcal{L}}^T(t){}^{\mathcal{T}}_{\mathcal{L}}\mathcal{R}(t)\mathbf{e}_3 = 0$, where $t \mapsto {}^{\mathcal{T}}_{\mathcal{L}}\mathcal{R}(t)\mathbf{e}_3$ may invert its direction. For this situation and in order to mimic a 2-D planning, one requires the follower third axis to be aligned with the leader's, i.e., $t \mapsto ({}^{\mathcal{T}}_{\mathcal{L}}\mathcal{R}(t)\mathbf{e}_3)^T {}^{\mathcal{T}}_{\mathcal{T}}\mathcal{R}(t)\mathbf{e}_3 = \pm 1$. For $t \mapsto {}^{\mathcal{T}}_{\mathcal{T}}\mathcal{R}(t)\mathbf{e}_3$ to be constant [$t \mapsto {}^{\mathcal{T}}_{\mathcal{L}}\mathcal{R}(t)\mathbf{e}_3$ is constant except for a sign change], the follower vehicle cannot roll nor pitch $({}^{\mathcal{T}}_{\mathcal{T}}\dot{\mathcal{R}}(t)\mathbf{e}_3 = q_{\mathcal{T}}(t){}^{\mathcal{T}}_{\mathcal{T}}\mathcal{R}(t)\mathbf{e}_1 - p_{\mathcal{T}}(t){}^{\mathcal{T}}_{\mathcal{T}}\mathcal{R}(t)\mathbf{e}_2 = 0 \Rightarrow p_{\mathcal{T}}(t) = q_{\mathcal{T}}(t) = 0)$. As a consequence and because $q_{\mathcal{T}}(t) \propto \mathbf{v}_{\mathcal{L}}^T(t){}^{\mathcal{T}}_{\mathcal{T}}\mathcal{R}(t)\mathbf{e}_3$ [see (6)], it follows that a possible choice for the roll rate should satisfy $p_{\mathcal{T}}(t) \propto \mathbf{v}_{\mathcal{L}}^T(t){}^{\mathcal{T}}_{\mathcal{T}}\mathcal{R}(t)\mathbf{e}_3$, where $\mathbf{v}_{\mathcal{L}}^T(t){}^{\mathcal{T}}_{\mathcal{T}}\mathcal{R}(t)\mathbf{e}_3$ is zero for a leader in a planar motion [${}^{\mathcal{T}}_{\mathcal{T}}\mathcal{R}(t)\mathbf{e}_3$ and ${}^{\mathcal{T}}_{\mathcal{L}}\mathcal{R}(t)\mathbf{e}_3$ are aligned and $\mathbf{v}_{\mathcal{L}}^T(t){}^{\mathcal{T}}_{\mathcal{L}}\mathcal{R}(t)\mathbf{e}_3 = 0$].

[5] In a 2-D setting, $\mathbf{r}_1$ lives in a closed space, specifically the unit circle.

With the previous comments in mind, the following roll rate is proposed:

$$p_{\mathcal{T}}(t) = \mathrm{s}^{\star(0)}(t)\frac{\mathbf{v}_{\mathcal{L}}^{T}(t){}_{\mathcal{T}}^{\mathcal{I}}\mathcal{R}(t)\mathbf{e}_3}{d_{\perp}} \tag{17}$$

where $\mathrm{s}^{\star(0)} \in \mathcal{C}^2(\mathbb{R}_{\geq 0}, [-1, 1])$ is a *modified signum function* that is obtained by solving the differential equation

$$\mathrm{s}^{\star(3)}(t) + a_2\,\mathrm{s}^{\star(2)}(t) + a_1\,\mathrm{s}^{\star(1)}(t) + a_0\,\mathrm{s}^{\star(0)}(t) = a_0\,\eta(t) \tag{18}$$

with coefficients $a_2 > 0$ and $a_2 a_1 > a_0$ to guarantee the stability of the differential equation and $\eta : \mathbb{R}_{\geq 0} \to \{-1, 1\}$ given by

$$\eta(t) \equiv \mathrm{sign}\left(\mathbf{n}^{T}{}_{\mathcal{T}}^{\mathcal{I}}\mathcal{R}(t)\mathbf{e}_3\right)\mathrm{sign}\left(\mathbf{v}_{\mathcal{L}}^{T}(t){}_{\mathcal{T}}^{\mathcal{I}}\mathcal{R}(t)\mathbf{e}_2\right) \tag{19}$$

and where $d_{\perp}$ can be viewed as the radius of a trailer spherical body with hinge point $\mathbf{p}_{\mathcal{T}}$ (see Fig. 1). The parameter $d_{\perp}$, provided by the designer, represents a sensitivity of the planning to the leader path torsion (similar to d, which is a sensitivity parameter for the leader path curvature).

At the equilibrium, $\mathrm{s}^{\star(0)}(\cdot) = \eta(\cdot) = \pm 1$, and $\eta(\cdot)$ plays an extremely important role on the stability analysis. The term $\mathrm{sign}\left(\mathbf{v}_{\mathcal{L}}^{T}(\cdot){}_{\mathcal{T}}^{\mathcal{I}}\mathcal{R}(\cdot)\mathbf{e}_2\right)$ in (19) guarantees that both $\mathcal{R}_1^{3D}$ and $\mathcal{R}_2^{3D}$ are stable, while the term $\mathrm{sign}\left(\mathbf{n}^{T}{}_{\mathcal{T}}^{\mathcal{I}}\mathcal{R}(\cdot)\mathbf{e}_3\right)$ in (19) guarantees that only the solution where the trailer stands up is stable.

Now, one should mention beforehand that if a *real* follower vehicle needs a position reference to be of class $\mathcal{C}^{(n)}$, then $t \mapsto \boldsymbol{\omega}_{\mathcal{F}}(t)$ must be of class $\mathcal{C}^{(n-1)}$ and, consequently, so does $t \mapsto p_{\mathcal{T}}(t)$. The proposed path planning solution is validated resorting to quadrotor vehicles, which require a position reference to be of class $\mathcal{C}^{(3)}$ (continuous position, velocity, acceleration and jerk); thus, $t \mapsto p_{\mathcal{T}}(t)$ must be of class $\mathcal{C}^{(2)}$, which explains why in (17) $t \mapsto \mathrm{s}^{\star(0)}(t)$ is used instead of $t \mapsto \eta(t)$ [η is discontinuous while $\mathrm{s}^{\star(0)}$ is of class $\mathcal{C}^{(2)}$ and, under certain conditions, $\lim_{t\to\infty}\mathrm{s}^{\star(0)}(t) = \lim_{t\to\infty}\eta(t) = \pm 1$].

As in Section VII, stability is first analyzed for a leader describing a trimming path and only afterward for a leader describing a nontrimming path.

B. Convergence for Trimming Paths

Note that the stability of $\mathbf{r}_1^{\star}(\boldsymbol{\kappa}_{\mathcal{L}}d)$ and the convergence of $t \mapsto \mathbf{r}_1(t)$ to $\mathbf{r}_1^{\star}(\boldsymbol{\kappa}_{\mathcal{L}}d)$ have been studied for any choice of $t \mapsto p_{\mathcal{T}}(t)$. The remaining subspace left unstudied is spanned by $t \mapsto \mathbf{r}_2(t)$ and $t \mapsto \mathbf{r}_3(t)$ [recall that $\mathcal{R} \equiv {}_{\mathcal{T}}^{\mathcal{L}}\mathcal{R} \equiv \left[\mathbf{r}_1\ \mathbf{r}_2\ \mathbf{r}_3\right] \equiv [\mathrm{r}_{ij}] \in \mathcal{SO}(3)$], which is the orthogonal space to $t \mapsto \mathbf{r}_1(t)$. From the kinematics of $t \mapsto \mathbf{r}_1(t)$ in (8), it follows that the orthogonal space to $t \mapsto \mathbf{r}_1(t)$ is fixed if $t \mapsto \mathbf{r}_1^{T}(t){}^{\mathcal{L}}\boldsymbol{\omega}_{\mathcal{T}|\mathcal{L}}(t) = 0$. This motivates the introduction of the error

$$z_2(t) = \mathbf{r}_1^{T}(t)\frac{{}^{\mathcal{L}}\boldsymbol{\omega}_{\mathcal{T}|\mathcal{L}}(t)}{v_{\mathcal{L}}(t)} = \frac{p_{\mathcal{T}}(t)}{v_{\mathcal{L}}(t)} - \mathbf{r}_1^{T}(t)\boldsymbol{\kappa}_{\mathcal{L}} \tag{20}$$

where $\boldsymbol{\kappa}_{\mathcal{L}}$ is constant for a trimming path. The error $t \mapsto z_2(t)$ relates the angular velocities of the leader and the follower along the direction $t \mapsto \mathbf{r}_1(t)$. Again, the error is velocity-independent, because convergence depends on the intrinsic properties of the path and not on the velocity with which the path is followed.

The equilibria of (7) are found by setting $\mathbf{z}(\cdot) = \mathbf{0}$ and $z_2(\cdot) = 0$, or equivalently by setting ${}^{\mathcal{L}}\boldsymbol{\omega}_{\mathcal{T}|\mathcal{L}}(\cdot) = \mathbf{0}$. Recall from Section VII-B that for the equilibrium solution $\mathbf{r}_1^{\star}(\boldsymbol{\kappa}_{\mathcal{L}}d)$, it follows that $\mathbf{r}_1^{\star\,T}(\boldsymbol{\kappa}_{\mathcal{L}}d)\boldsymbol{\kappa}_{\mathcal{L}} = (\tau_{\mathcal{L}}/\mathrm{r}_{11}^{\star}(\boldsymbol{\kappa}_{\mathcal{L}}d))$. Moreover, if $\mathrm{s}^{\star(0)}(\cdot) = \eta(\cdot) = \pm 1$, and given the roll rate defined in (17), it follows from $z_2(\cdot) = 0$ that

$$\mathrm{r}_{31}^{\star}(\boldsymbol{\kappa}_{\mathcal{L}}d) = \eta\frac{\tau_{\mathcal{L}}d_{\perp}}{\mathrm{r}_{11}^{\star}(\boldsymbol{\kappa}_{\mathcal{L}}d)} \equiv \eta\frac{\tau_{\mathcal{L}}d}{\mathrm{r}_{11}^{\star}(\boldsymbol{\kappa}_{\mathcal{L}}d)}\lambda_{\mathrm{yz}}$$

where $\lambda_{\mathrm{yz}} \equiv (d_{\perp}/d)$. It can be proved that the equilibrium rotation matrix $\mathcal{R}^{\star}(\boldsymbol{\kappa}_{\mathcal{L}}d, \lambda_{\mathrm{yz}})$ exists if $\|\boldsymbol{\kappa}_{\mathcal{L}}d\| < \|\boldsymbol{\kappa}_{\mathcal{L}}d\|_{\max}$, where [29]

$$\|\boldsymbol{\kappa}_{\mathcal{L}}d\|_{\max}^2 = \frac{\lambda_{\mathrm{yz}}+1}{2}\left(\sqrt{1+\frac{(2\kappa_{\mathcal{L}}d)^2}{\lambda_{\mathrm{yz}}}} - 1\right). \tag{21}$$

This result is related to the fact that an equilibrium solution exists if and only if $\sup_{t\geq 0}(\|\boldsymbol{\omega}_{\mathcal{F}}(t)\|/v_{\mathcal{L}}(t)) \geq (\boldsymbol{\omega}_{\mathcal{L}}(\cdot)/v_{\mathcal{L}}(\cdot)) = \boldsymbol{\kappa}_{\mathcal{L}}$: if this condition is not verified, then $t \mapsto {}^{\mathcal{L}}\boldsymbol{\omega}_{\mathcal{T}|\mathcal{L}}(t) = \mathcal{R}(t)\boldsymbol{\omega}_{\mathcal{F}}(t) - \boldsymbol{\omega}_{\mathcal{L}}(t)$ cannot converge to $\mathbf{0}$. We emphasize that (21) can be made arbitrarily large, by selecting $d_{\perp}$ arbitrarily small.

If $(\kappa_{\mathcal{L}}d)^2 \leq (\kappa_{\mathcal{L}}^{\max}d)^2 < 1$ and $\|\boldsymbol{\kappa}_{\mathcal{L}}d\| < \|\boldsymbol{\kappa}_{\mathcal{L}}d\|_{\max}$, then an equilibrium matrix $\mathcal{R}^{\star}(\boldsymbol{\kappa}_{\mathcal{L}}d, \lambda_{\mathrm{yz}})$ exists. For brevity, only the terms $\mathbf{r}_1^{\star}(\boldsymbol{\kappa}_{\mathcal{L}}d)$ and $\mathrm{r}_{33}^{\star}(\boldsymbol{\kappa}_{\mathcal{L}}d, \lambda_{\mathrm{yz}})$ are presented, the former in (10) and the latter presented next

$$\mathrm{r}_{33}^{\star} = \mathrm{sign}\left(\mathrm{r}_{21}^{\star}\right)\left(-\frac{\tau_{\mathcal{L}}}{\kappa_{\mathcal{L}}}\frac{\tau_{\mathcal{L}}d}{\mathrm{r}_{11}^{\star}}\lambda_{\mathrm{yz}} + \sqrt{1+\frac{\tau_{\mathcal{L}}^2}{\kappa_{\mathcal{L}}^2}\left(1+\frac{1-\lambda_{\mathrm{yz}}}{\mathrm{r}_{11}^{\star 2}}\right)}\right). \tag{22}$$

As expected, for planar paths, when $\tau_{\mathcal{L}} = 0$, $\mathrm{r}_{33}^{\star}(\boldsymbol{\kappa}_{\mathcal{L}}d, \lambda_{\mathrm{yz}}) = \mathrm{sign}\left(\mathrm{r}_{21}^{\star}(\boldsymbol{\kappa}_{\mathcal{L}}d, \lambda_{\mathrm{yz}})\right)$. The stable $\mathrm{r}_{33}^{\star}(\boldsymbol{\kappa}_{\mathcal{L}}d, \lambda_{\mathrm{yz}})$ is either 1 or -1, because the leader Frenet reference frame may invert its third axis, but the stable trailer should always stand up (or down) [the stable $\mathrm{r}_{33}^{\star}(\boldsymbol{\kappa}_{\mathcal{L}}d, \lambda_{\mathrm{yz}})$ inverts sign when the leader's third axis inverts its direction].

A critical situation arises when $\mathrm{r}_{21}^{\star}(\boldsymbol{\kappa}_{\mathcal{L}}d, \lambda_{\mathrm{yz}}) = 0$. This is the case when $\|\boldsymbol{\kappa}_{\mathcal{L}}d\| = \|\boldsymbol{\kappa}_{\mathcal{L}}d\|_{\max}$ or when a leader describes a rectilinear path. For the latter situation, $\boldsymbol{\kappa}_{\mathcal{L}}d = \mathbf{0}$, and therefore, $\mathbf{r}_1^{\star}(\mathbf{0}) = \mathbf{e}_1$ and $\mathrm{r}_{21}^{\star}(\mathbf{0}) = 0$. Therefore, for a leader describing a rectilinear path, the condition $\mathrm{r}_{21}^{\star}(\mathbf{0}) \neq 0$ does not hold and $z_2(\cdot) = 0$ is satisfied for $\mathcal{R}^{\star}(\mathbf{0}) = \mathcal{R}_x(\phi)$ for all $\phi \in \mathbb{R}$. For a leader describing a rectilinear path, the existence of infinite equilibria is understandable, because there is no preferable plane to converge to (i.e., the plane of motion of the leader can be any whose normal is perpendicular to $t \mapsto {}_{\mathcal{L}}^{\mathcal{I}}\mathcal{R}(t)\mathbf{e}_1 = \text{constant}$).

For a trimming path, two equilibrium solutions for (8) exist, namely $\mathbf{r}_1^{\star}(\boldsymbol{\kappa}_{\mathcal{L}}d)$ and $\bar{\mathbf{r}}_1^{\star}(\boldsymbol{\kappa}_{\mathcal{L}}d)$, with $\mathbf{r}_1^{\star}(\boldsymbol{\kappa}_{\mathcal{L}}d)$ being an AGAS equilibrium of (8). Thus, (7) has four equilibrium solutions: two of those are associated with $\bar{\mathbf{r}}_1^{\star}(\boldsymbol{\kappa}_{\mathcal{L}}d)$ and, as a consequence, are unstable; the other two are associated with $\mathbf{r}_1^{\star}(\boldsymbol{\kappa}_{\mathcal{L}}d)$ and it is the objective of this section to prove that one of those is stable with the other being unstable.

Theorem 5: Consider a leader vehicle describing a trimming path and a trailer with kinematics (6) and (17). If $\mathbf{r}_1(0) \in \mathcal{S}^2\backslash\{\bar{\mathbf{r}}_1^{\star}\}$, $0 < (\kappa_{\mathcal{L}}d) < 1$ and $\|\boldsymbol{\kappa}_{\mathcal{L}}d\| < \|\boldsymbol{\kappa}_{\mathcal{L}}d\|_{\max}$, then the trailer reference frame system as described by (7) has an asymptotically stable equilibrium point.

The proof follows from analyzing the dynamics of the error z_2 in (20) and showing that z_2 vanishes asymptotically;

this in turn implies that $\mathbf{z}$ also vanishes asymptotically and that the trailer reference frame has an asymptotically stable equilibrium point (details found in [29]).

C. Convergence for Nontrimming Paths

Theorem 5 states that an asymptotically stable equilibrium solution $\mathcal{R}^{\star}(\cdot,\cdot)$ exists, but [similar to $\mathbf{r}_1^{\star}(\cdot)$] it is only valid for the trimming paths. Thus, once again, the question is raised of whether a unique rotation matrix exists, which depends solely on the leader's path intrinsic properties and on the planner specifications (d, $d_{\perp}$, and $\mathbf{n}$). Next, we show that (7) has an attracting solution and that all the solutions starting sufficiently close to the attracting solution converge to that attracting solution (once again, we refer to contraction analysis [31]).

Theorem 6: Consider a leader vehicle and a trailer with kinematics (6) and (17). Assume that $0 < (\kappa_{\mathcal{L}}(t)d)^2 < 1$ and that $\|\boldsymbol{\kappa}_{\mathcal{L}}(t)d\| < \|\boldsymbol{\kappa}_{\mathcal{L}}d\|_{\max}$ for all $t \geq 0$, and that $\mathbf{r}_1(0) \in \Omega_1(0)$. Then, if a solution $t \mapsto \mathcal{R}(t)$ to (7) exists, where $\inf_{t\geq 0} \mathrm{r}_{21}(t) > 0$ and $\inf_{t\geq 0} \operatorname{sign}\left(\mathbf{n}^T {}^{\mathcal{I}}_{\mathcal{F}}\mathcal{R}(t)\mathbf{e}_3\right) > 0$, then (7) has a locally attracting solution.

Theorem 6 guarantees that for n *virtual* follower vehicles computing $t \mapsto {}^{\mathcal{I}}_{\mathcal{T}}\mathcal{R}(t)$ independently, all rotation matrices converge to one another. Its proof follows the same spirit as that of Theorem 2, and it is found in [29].

D. Duality and Simulation

There are specific tasks that require a group of vehicles to move in a fixed geometrical formation along a predefined path, which is guided by a leader, as in the framework proposed in this article. Then, a relevant question is what motion should be imposed on a leader in order to satisfy that objective. This question has a straightforward answer if we consider the dual problem of that of finding the trailer motion, given a leader motion. Indeed, by imposing a motion to a trailer reference frame, the leader motion is determined with the help of (4).

As such, if we want the formation leader+followers to move with the orientation of an arbitrary path, we set the trailer position to be the path position and the trailer longitudinal axis to be the path tangent. We can then command the leader to describe the trajectory that would follow from (4) and Theorems 2 and 6 guarantee that an attracting solution exists, meaning that all the followers can perform the planning independently and they converge to the same trailer reference frame that was used to construct the leader motion.

In Fig. 5, we present a simulation where a leader describes a helix path and three followers are attached to the leader: the design specifications are $d = 0.15\,\mathrm{m}$, $d_{\perp} = 0.15\,\mathrm{m}$ and $\mathbf{n} = \mathbf{e}_3$; also the distances $\bar{\mathbf{d}}$ for the three followers are chosen to be $0.2\{[0\,(1/2)\,-((3)^{1/2}/6)], [0\,-(1/2)\,-((3)^{1/2}/6)], [0\,0\,((3)^{1/2}/3)]\}\,\mathrm{m}$ and, with this choice, the configuration forms a pyramid with a base formed by the three followers (corners of an equilateral triangle of length 0.2 m and the leader at the vertex of the pyramid). Fig. 5(a) shows the trajectories for the first 3 s of the simulation and note that, at its initial state, the formation does not form the desired pyramid; however, by the end, the formation already resembles the desired pyramid.

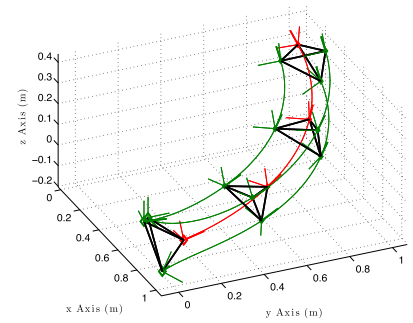

(a)

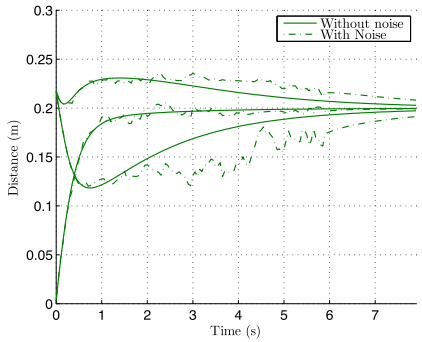

(b)

Fig. 5. Leader-and-3-follower formation for a leader describing a helix path. (a) Perspective 1: leader in red and followers in green with positions sampled four times (◇ for initial positions) (only first 3 s). (b) Distance between followers, with and without noise (noise turned off after 6 s).

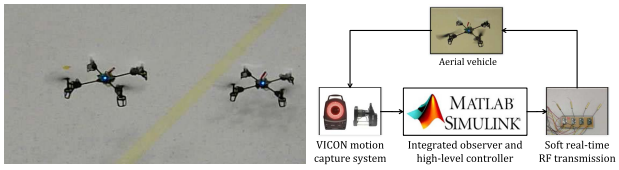

Fig. 6. Left: leader–follower formation with quadrotor vehicles. Right: quadrotor control architecture.

In Fig. 5(b), the distance between followers is presented for the first 8 s and the convergence of all the distances to 0.2 m (full lines) is clear. In order to attest the robustness of the planning, another simulation was performed where the velocity measurements used by each follower are corrupted with noise (independent noise for each follower) for the first 6 s: in Fig. 5(b) (dashed lines), the distance between followers is presented for the first 8 s and note that the convergence of all distances to 0.2 m is still clear. Note that a corrupted velocity affects the kinematics of the planner, but Theorems 2 and 6 guarantee that an attracting solution exists, which is why noise in the velocity measurements does not have a permanent effect on the planning; in fact, when the noise is switched off, normal convergence is recovered.

A hard problem, which we do not address in this article, is to decide when should the vehicles exchange information and negotiate their relative motions. This problem needs to be addressed in an environment where obstacle avoidance is

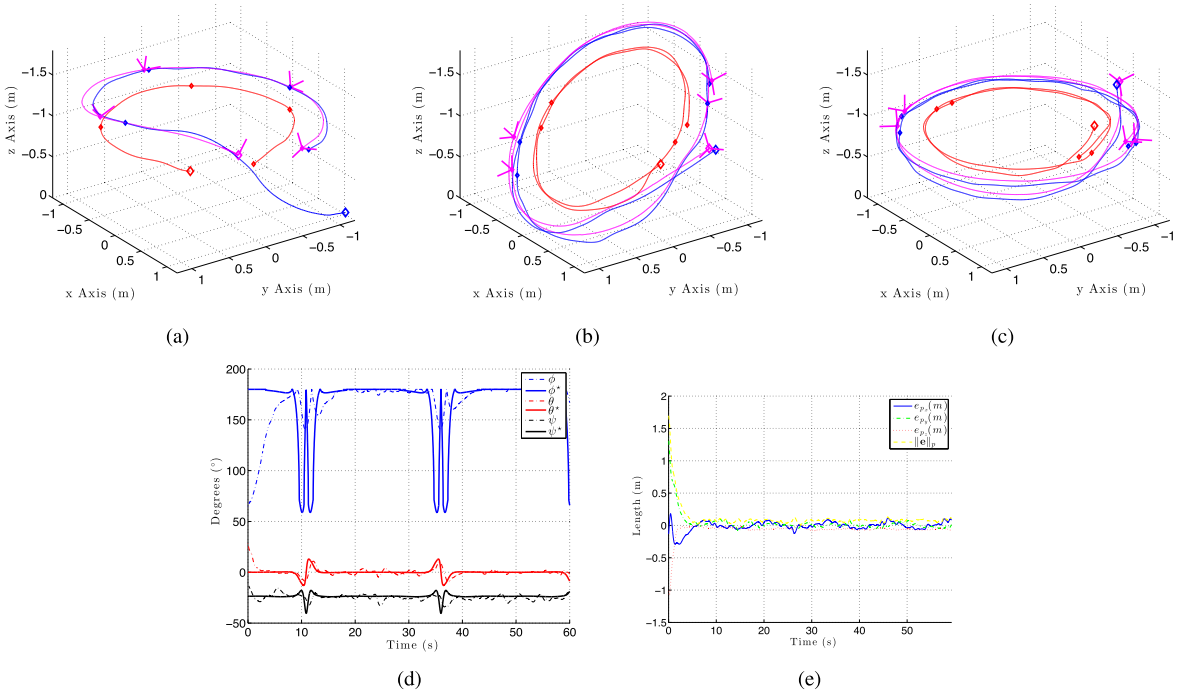

Fig. 7. Leader describing circular paths with 1-m radius and changing from horizontal plane to the plane tilted by 45°. (a) From 0 to 11 s. (b) From 11 to 35 s. (c) From 35 to 61 s. (d) Euler angles for $\mathcal{R}$ and for $\mathcal{R}^{\star}$. (e) Position-tracking error between *virtual* and *real* followers.

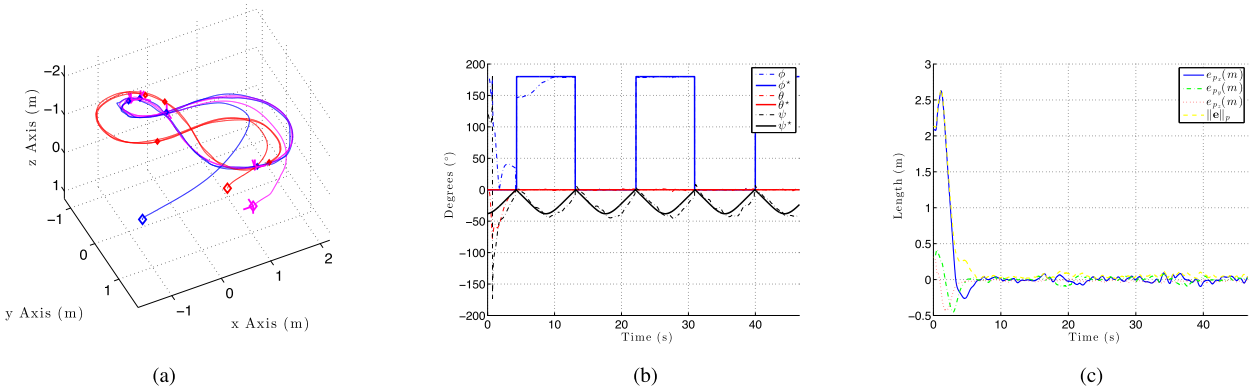

Fig. 8. Leader describing a lemniscate path. (a) Vehicles' trajectories. (b) Euler angles for $\mathcal{R}$ and for $\mathcal{R}^{\star}$. (c) Position-tracking error between the *virtual* and *real* followers.

required, in which case a fixed configuration might have to be broken in order to avoid collisions. For these situations, our suggestion is for the vehicles to use a time-varying $t \mapsto \bar{\mathbf{d}}(t)$ and communicate it to their peers. For this situation, the followers would behave as moving points belonging to a common moving frame (the trailer frame), e.g., for three followers [as in Fig. 5(a)] instead of a fixed pyramid moving in a helix-shaped trajectory, we would obtain a time-varying pyramid moving in an helix-shaped trajectory. Obviously, an extra step is required to plan the time evolution of the relative positions, which requires communication among vehicles. This problem is outside the scope of this article and we have not developed a solution to such problem. It is a topic left for future research.

IX. Experimental Validation

This section presents the experimental results obtained at the Sensor-Based Cooperative Robotics Research Laboratory—SCORE Lab—of the Faculty of Science and Technology of the University of Macau. For the experimental validation of the proposed algorithm, we employed the architecture shown in Fig. 6, where an MATLAB/Simulink environment is used to integrate the sensors, the control algorithm, and the communication with the vehicle seamlessly. The proposed trajectory planner was tested with two radio-controlled Blade mQX quadrotor vehicles [32], as shown in Fig. 6. A VICON T-Series motion capture system [33], composed of 12 T-Series cameras and markers attached to the quadrotors, provides highly accurate position and orientation measurements for the leader and follower at a rate of 100 Hz. The trajectory planner is implemented in an MATLAB/Simulink model, which computes the follower's position reference and feeds it to the quadrotors's trajectory tracker controller developed in [34], which requires a time-parameterized position reference of class $\mathcal{C}^{(3)}$. Consequently, the trajectory planner requires the knowledge of $\mathbf{p}_{\mathcal{L}}^{(i)}(t)$ for $i = \{1, 2, 3\}$, which are obtained

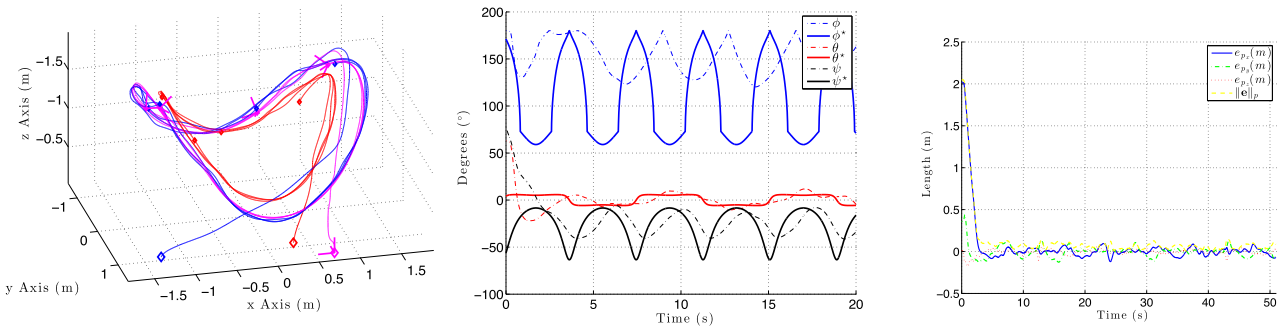

(a) (b) (c)

Fig. 9. Leader describing a circle in a horizontal plane with sinusoidal altitude variation. (a) Vehicles' trajectories. (b) Euler angles for $\mathcal{R}$ and for $\mathcal{R}^\star$. (c) Position-tracking error between the *virtual* and *real* followers.

from the raw position measurements by means of dynamic differentiators.

In all the experimental results presented in the sequel, the leader's path is depicted in red, the real follower's path in blue, and the *virtual* follower's path in magenta, with the magenta reference frame being that of the *virtual follower*, i.e., ${}^{\mathcal{I}}_{\mathcal{F}}\mathcal{R}(\cdot)$ [see Figs. 7(a)–(c), 8(a), and 9(a)]. In the figures, the vehicles' positions are shown five times, with $\diamond$ symbol for the initial position and $\bullet$ symbol for the other positions, equally spaced in time (experiment time divided by 4). Finally, in all the experiments, the leader's velocity was set at 0.5 ms^{-1}, $\mathbf{n}$ was set to $\mathbf{e}_3$, and the position tracking error obtained with the controller in [34] is also presented.

Consider the xyz Euler angles for attitude parameterization, defined such that $\mathcal{R} := \mathcal{R}_z(\psi)\mathcal{R}_y(\theta)\mathcal{R}_x(\phi)$ and $\mathcal{R}^\star := \mathcal{R}_z(\psi^\star)\mathcal{R}_y(\theta^\star)\mathcal{R}_x(\phi^\star)$. We have shown that if the leader describes a trimming path, the relative position between the leader and the follower $t \mapsto {}^{\mathcal{L}}\mathbf{p}_{\mathcal{F}|\mathcal{L}}(t) = -\mathcal{R}(t)\mathbf{d}$ converges to ${}^{\mathcal{L}}\mathbf{p}^\star_{\mathcal{F}|\mathcal{L}}(\kappa_{\mathcal{L}}d, \lambda_{\text{yz}}) = -\mathcal{R}^\star(\kappa_{\mathcal{L}}d, \lambda_{\text{yz}})\mathbf{d}$, with $\kappa_{\mathcal{L}}$ and $\tau_{\mathcal{L}}$ as the constant leader's path curvature and torsion. For nontrimming paths, the matrix $t \mapsto \mathcal{R}(t)$ is expected to remain close to the matrix $t \mapsto \mathcal{R}^\star(\kappa_{\mathcal{L}}(t)d, \lambda_{\text{yz}})$, where $t \mapsto \kappa_{\mathcal{L}}(t), \tau_{\mathcal{L}}(\cdot)$ are time-varying. For all experiments, $\{\phi(\cdot), \theta(\cdot), \psi(\cdot)\}$ and $\{\phi^\star(\cdot), \theta^\star(\cdot), \psi^\star(\cdot)\}$ are presented in dashed and full lines, respectively. $\{\phi^\star(\cdot), \theta^\star(\cdot), \psi^\star(\cdot)\}$ are determined using formulas (10) and (22); $\{\phi(\cdot), \theta(\cdot), \psi(\cdot)\}$ are determined from $\mathcal{R}(\cdot) := {}^{\mathcal{L}}_{\mathcal{I}}\mathcal{R}(\cdot){}^{\mathcal{I}}_{\mathcal{F}}\mathcal{R}(\cdot)$. Moreover, for all the experiments, $\{a_0, a_1, a_2\} = \{152, 72, 12\}$ in (18).

Fig. 7 shows the vehicle paths for an experiment performed with $d = d_\perp = 0.4\,\text{m}$, relative position vector $\bar{\mathbf{d}} = \begin{bmatrix}0 & -0.4 & 0\end{bmatrix}^T\text{m}$, and the quadrotor-leader describing a path composed of two circular paths: one in a horizontal plane and the other in a plane tilted by 45°. The leader's path has zero torsion for most of the path, except during the transition between planes. Note the convergence of the *virtual* follower's path to a zero-torsion path in the leader's plane of motion, since $\mathbf{e}_3^T\bar{\mathbf{d}} = 0$. Except during the transition between planes, the leader describes the trimming paths, and for that reason, $\{\phi(\cdot), \theta(\cdot), \psi(\cdot)\}$ converge to $\{\phi^\star(\cdot), \theta^\star(\cdot), \psi^\star(\cdot)\}$, which are constant. In addition, the *virtual* follower's third axis ${}^{\mathcal{I}}_{\mathcal{F}}\mathcal{R}(\cdot)\mathbf{e}_3$ remains aligned with $\mathbf{n}$, i.e., sign $\left(\mathbf{n}^T\,{}^{\mathcal{I}}_{\mathcal{F}}\mathcal{R}(\cdot)\mathbf{e}\right) > 0$.

The quadrotor paths for $d = d_\perp = 0.35\,\text{m}$, relative position vector $\bar{\mathbf{d}} = \begin{bmatrix}0 & 0.35 & 0\end{bmatrix}^T\text{m}$ and the quadrotor-leader describing a lemniscate path in a horizontal plane are shown in Fig. 8. The lemniscate is defined in meters as

$$\mathbf{p}(\gamma) = 1.7\,\mathcal{R}_z\left(-\frac{\pi}{4}\right)\left[\frac{\cos(\gamma)}{1+\sin^2(\gamma)} \;\; \frac{1}{2}\frac{\sin(2\gamma)}{1+\sin^2(\gamma)} \;\; -1.1\right]^T$$

with $\dot{\gamma}(t) = (0.5/1.7)(1 + \sin^2(\gamma(t)))^{1/2}$ to normalize the trajectory velocity to $0.5\,\text{ms}^{-1}$. The leader's path has zero torsion and, once again, the *virtual* follower converges to a plane parallel to the leader's plane of motion, without any prior knowledge that the leader is moving in that plane. In Fig. 8(b), the time evolution of the angles $\{\phi(\cdot), \theta(\cdot), \psi(\cdot)\}$ and $\{\phi^\star(\cdot), \theta^\star(\cdot), \psi^\star(\cdot)\}$ is presented. The leader does not describe a trimming path and, consequently, $\{\phi^\star(\cdot), \theta^\star(\cdot), \psi^\star(\cdot)\}$ vary with time. Note that $\psi(\cdot)$ follows $\psi^\star(\cdot)$ with a certain delay; $\theta(\cdot)$ and $\theta^\star(\cdot)$ are zero, because the trajectory is planar; and $\phi(\cdot)$ and $\phi^\star(\cdot)$ switch between 0° and 180° for clockwise and anticlockwise rotations, respectively. When the leader describes an almost rectilinear trajectory, ${}^{\mathcal{I}}_{\mathcal{L}}\mathcal{R}(\cdot)$ is ill-defined and we set $\{\phi(\cdot), \theta(\cdot), \psi(\cdot)\} = \{\phi^\star(\cdot), \theta^\star(\cdot), \psi^\star(\cdot)\} = \{0, 0, 0\}$. The direction ${}^{\mathcal{I}}_{\mathcal{F}}\mathcal{R}(\cdot)\mathbf{e}_3$ is aligned with $\mathbf{n}$, i.e., sign $\left(\mathbf{n}^T{}^{\mathcal{I}}_{\mathcal{F}}\mathcal{R}(\cdot)\mathbf{e}_3\right) > 0$, and the follower's curvature is smaller than the leader's when the leader's rotation is clockwise and larger when the leader's rotation is anticlockwise.

Finally, Fig. 9 shows the quadrotor's paths for $d = d_\perp = 0.4\,\text{m}$, $\bar{\mathbf{d}} = [0\ 0.4\ 0]^T$ m and a quadrotor-leader describing the trajectory (in meters)

$$\mathbf{p}(\gamma) = \begin{bmatrix}\sin(\gamma) & \cos(\gamma) & 0.5\cos(\gamma) - 1\end{bmatrix}^T$$

with $\dot{\gamma}(t) = 0.5(1/(2(3 - \cos(4\gamma(t)))))^{1/2})\text{s}^{-1}$. The leader's path is not planar, but the *virtual* follower, which behaves like a *3-D trailer* attached to the leader, is at each moment compeled to remain in the osculating plane of the leader [spanned by ${}^{\mathcal{I}}_{\mathcal{L}}\mathcal{R}(\cdot)\mathbf{e}_1$ and ${}^{\mathcal{I}}_{\mathcal{L}}\mathcal{R}(\cdot)\mathbf{e}_2$]. In Fig. 9(b), the time evolution of the angles $\{\phi(\cdot), \theta(\cdot), \psi(\cdot)\}$ and $\{\phi^\star(\cdot), \theta^\star(\cdot), \psi^\star(\cdot)\}$, which is periodic, is only presented from 0 to 20 s. The trajectory is not a trimming one and, once again, the angles $\{\phi(\cdot), \theta(\cdot), \psi(\cdot)\}$ try to follow $\{\phi^\star(\cdot), \theta^\star(\cdot), \psi^\star(\cdot)\}$ but with a certain delay.

A video of an experiment similar to that in Fig. 7 is found in [35]. The presented experiments illustrate a formation

between a leader and a single follower. For formations between a leader and several followers, we refer the reader to the simulations shown in Fig. 5, illustrating a leader and three followers that asymptotically come together in a pyramid formation (with the leader at the vertex of the pyramid). Both the experiments and the simulations illustrate the robustness of the planning algorithm against measurement noise. Other types of disturbances, such as unknown wind forces acting on the quadrotors or unknown model parameters, must be handled by the trajectory-tracking controller: in our experiments, we made use of the controller described in [34], but other controllers, with different types of robustness guarantees, can be used.

X. Conclusion

In this article, we presented a real-time 3-D trajectory planner for leader following, where n followers asymptotically behave as n distinct points of a common 3-D trailer reference frame. The proposed trajectory planner produces natural trajectories for the followers that are not mere offset copies of the leader's trajectory, and it can be implemented independently by each follower, thus reducing the need for communications among vehicles. We proved that under a wide range of conditions, there is a unique attractive solution for the trailer reference frame to which all solutions converge to, which demonstrates the robustness of the planning to noisy measurements and different initializations. The formation of $n + 1$ vehicles is driven by the leader, and we have discussed how to obtain a leader trajectory that renders a desired formation asymptotically stable. Experiments performed with quadrotor vehicles were conducted that demonstrate the richness and suitability of the generated trajectories. Directions for future work include the study of a sequence of n-trailers and the incorporation of a collision avoidance strategy.

References

[1] J. Fink, N. Michael, S. Kim, and V. Kumar, "Planning and control for cooperative manipulation and transportation with aerial robots," *Int. J. Robot. Res.*, vol. 30, no. 3, pp. 324–334, Mar. 2011.

[2] T. Arai and J. Ota, "Dwarf intelligence—A large object carried by seven dwarves," *Robot. Auton. Syst.*, vol. 18, no. 1, pp. 149–155, Jul. 1996.

[3] J. G. Bellingham and K. Rajan, "Robotics in remote and hostile environments," *Science*, vol. 318, pp. 1098–1102, Nov. 2007.

[4] N. E. Leonard, D. A. Paley, R. E. Davis, D. M. Fratantoni, F. Lekien, and F. M. Zhang, "Coordinated control of an underwater glider fleet in an adaptive ocean sampling field experiment in Monterey Bay," *J. Field Robot.*, vol. 27, no. 6, pp. 718–740, Nov. 2010.

[5] Z. Peng, G. Wen, A. Rahmani, and Y. Yu, "Distributed consensus-based formation control for multiple nonholonomic mobile robots with a specified reference trajectory," *Int. J. Syst. Sci.*, vol. 46, no. 8, pp. 1447–1457, Jun. 2015.

[6] T. Balch and R. C. Arkin, "Behavior-based formation control for multirobot teams," *IEEE Trans. Robot. Autom.*, vol. 14, no. 6, pp. 926–939, Dec. 1998.

[7] J. R. T. Lawton, R. W. Beard, and B. J. Young, "A decentralized approach to formation maneuvers," *IEEE Trans. Robot. Autom.*, vol. 19, no. 6, pp. 933–941, Dec. 2003.

[8] G. Antonelli, E. Arrichiello, and S. Chiaverini, "Experiments of formation control with multirobot systems using the null-space-based behavioral control," *IEEE Trans. Control Syst. Technol.*, vol. 17, no. 5, pp. 1173–1182, Sep. 2009.

[9] K. Sugihara and I. Suzuki, "Distributed algorithms for formation of geometric patterns with many mobile robots," *J. Robot. Syst.*, vol. 13, no. 3, pp. 127–139, 1996.

[10] R. W. Beard, J. Lawton, and F. Y. Hadaegh, "A feedback architecture for formation control," in *Proc. Amer. Control Conf.*, vol. 6, Jun. 2000, pp. 4087–4091.

[11] K. D. Do and J. Pan, "Nonlinear formation control of unicycle-type mobile robots," *Robot. Auton. Syst.*, vol. 55, no. 3, pp. 191–204, 2007.

[12] S. S. Ge, X. Liu, C.-H. Goh, and L. Xu, "Formation tracking control of multiagents in constrained space," *IEEE Trans. Control Syst. Technol.*, vol. 24, no. 3, pp. 992–1003, May 2016.

[13] M. Egerstedt, X. Hu, and A. Stotsky, "Control of mobile platforms using a virtual vehicle approach," *IEEE Trans. Autom. Control*, vol. 46, no. 11, pp. 1777–1782, Nov. 2001.

[14] V. Roldão, R. Cunha, D. Cabecinhas, C. Silvestre, and P. Oliveira, "A leader-following trajectory generator with application to quadrotor formation flight," *Robot. Auton. Syst.*, vol. 62, pp. 1597–1609, Oct. 2014.

[15] R. Cui, S. S. Ge, B. V. E. How, and Y. S. Choo, "Leader–follower formation control of underactuated autonomous underwater vehicles," *Ocean Eng.*, vol. 37, pp. 1491–1502, Dec. 2010.

[16] Z. Peng, G. Wen, A. Rahmani, and Y. Yu, "Leader–follower formation control of nonholonomic mobile robots based on a bioinspired neurodynamic based approach," *Robot. Auto. Syst.*, vol. 61, no. 9, pp. 988–996, Sep. 2013.

[17] Y. Gu *et al.*, "Design and flight testing evaluation of formation control laws," *IEEE Trans. Control Syst. Technol.*, vol. 14, no. 6, pp. 1105–1112, Nov. 2006.

[18] G. Mariottini, F. Morbidi, D. Prattichizzo, G. J. Pappas, and K. Daniilidis, "Leader-follower formations: Uncalibrated vision-based localization and control," in *Proc. IEEE Int. Conf. Robot. Automat.*, Apr. 2007, pp. 2403–2408.

[19] A. K. Das, R. Fierro, V. Kumar, J. P. Ostrowski, J. Spletzer, and C. J. Taylor, "A vision-based formation control framework," *IEEE Trans. Robot. Autom.*, vol. 18, no. 5, pp. 813–825, Oct. 2002.

[20] R. W. Beard, J. Lawton, and F. Y. Hadaegh, "A coordination architecture for spacecraft formation control," *IEEE Trans. Control Syst. Technol.*, vol. 9, no. 6, pp. 777–790, Nov. 2001.

[21] L. Consolini, F. Morbidi, D. Prattichizzo, and M. Tosques, "Leader–follower formation control of nonholonomic mobile robots with input constraints," *Automatica*, vol. 44, no. 5, pp. 1343–1349, May 2008.

[22] S. Mastellone, D. M. Stipanovic, C. R. Graunke, K. A. Intlekofer, and M. W. Spong, "Formation control and collision avoidance for multi-agent non-holonomic systems: Theory and experiments," *Int. J. Robot. Res.*, vol. 27, no. 1, pp. 107–126, 2008.

[23] B. Hu and M. D. Lemmon, "Distributed switching control to achieve almost sure safety for leader-follower vehicular networked systems," *IEEE Trans. Autom. Control*, vol. 60, no. 12, pp. 3195–3209, Dec. 2015.

[24] N. E. Leonard and E. Fiorelli, "Virtual leaders, artificial potentials and coordinated control of groups," in *Proc. 40th IEEE Conf. Decis. Control*, vol. 3. Dec. 2001, pp. 2968–2973.

[25] E. W. Justh and P. S. Krishnaprasad, "Equilibria and steering laws for planar formations," *Syst. Control Lett.*, vol. 52, no. 1, pp. 25–38, May 2004.

[26] L. Consolini, F. Morbidi, D. Prattichizzo, and M. Tosques, "On the control of a leader-follower formation of nonholonomic mobile robots," in *Proc. 45th IEEE Conf. Decis. Control*, Dec. 2006, pp. 5992–5997.

[27] M.-D. Hua, T. Hamel, P. Morin, and C. Samson, "Introduction to feedback control of underactuated VTOLvehicles: A review of basic control design ideas and principles," *IEEE Control Syst. Mag.*, vol. 33, no. 1, pp. 61–75, Feb. 2013.

[28] P. Pereira, D. Cabecinhas, R. Cunha, C. Silvestre, and P. Oliveira, "Three dimensional trajectory planner for real time leader following," in *Proc. IEEE Int. Conf. Robot. Automat. (ICRA)*, May/Jun. 2014, pp. 6561–6566.

[29] P. Pereira, D. Cabecinhas, R. Cunha, C. Silvestre, and P. Oliveira. *Complements to 'Real Time Three Dimensional Leader Following'*. Accessed: Jan. 2, 2015. [Online]. Available: https://fenix.tecnico.ulisboa.pt/homepage/ist165008/publications

[30] A. J. Hanson and H. Ma, "Parallel transport approach to curve framing," Indiana Univ. Bloomington, Bloomington, IN, USA, Tech. Rep. TR425, 1995.

[31] W. Lohmiller and J.-J. E. Slotine, "On contraction analysis for non-linear systems," *Automatica*, vol. 34, no. 6, pp. 683–696, 1998.

[32] *Quadrotor Specifications*, BlademQX, Dubai, UAE, Sep. 2013.

[33] *Vicon System*, VICON, Hauppauge, NY, USA, Sep. 2013.

[34] D. Cabecinhas, R. Cunha, and C. Silvestre, "A nonlinear quadrotor trajectory tracking controller with disturbance rejection," *Control Eng. Pract.*, vol. 21, pp. 1–10, May 2014.

[35] *Video*. Accessed: Apr. 2, 2018. [Online]. Available: http://users.isr.ist.utl.pt/~rmac/SCARVE/videos/ExperimentVideo.m4v

Pedro Pereira received the M.Sc. degree in aerospace engineering from the Instituto Superior Técnico (IST), Lisbon, Portugal, and the Delft University of Technology (TU Delft), Delft, The Netherlands, in 2013, and the Ph.D. degree from the Department of Automatic Control, KTH Royal Institute of Technology, Stockholm, Sweden, in 2019.

His current research interests include nonlinear control and motion planning for aerial vehicles.

Rita Cunha received the Licenciatura degree in information systems and computer engineering and the Ph.D. degree in electrical and computer engineering from the Instituto Superior Técnico (IST), Universidade de Lisboa, Lisbon, Portugal, in 1998 and 2007, respectively.

She is currently an Assistant Researcher with the Institute for Systems and Robotics, LARSyS, Lisbon, and an Invited Assistant Professor with the Department of Electrical and Computer Engineering, IST. Her current research interests include nonlinear systems and control, and vision- and laser-based control with application to autonomous air vehicles.

David Cabecinhas received the Licenciatura and Ph.D. degrees in electrical and computer engineering from the Instituto Superior Técnico, Lisbon, Portugal, in 2006 and 2014, respectively.

He has been a Researcher with the Laboratory of Robotics and Systems in Engineering and Science, Institute for Systems and Robotics, Lisbon, since 2007. He is currently a Post-Doctoral Fellow with the Faculty of Science and Technology, University of Macau, Macau, China. His current research interests include nonlinear control, sensor- and vision-based control with applications to autonomous aerial and surface vehicles, and modeling and identification of aerial and surface vehicles.

Carlos Silvestre received the Licenciatura and M.Sc. degrees in electrical engineering and the Ph.D. degree in control science from the Instituto Superior Técnico (IST), Lisbon, Portugal, in 1987, 1991, and 2000, respectively, and the Habilitation degree in electrical engineering and computers from IST.

Since 2000, he has been with the Department of Electrical Engineering, IST, where he is currently an Associate Professor of control and robotics on leave. Since 2015, he has been a Professor with the Department of Electrical and Computers Engineering, Faculty of Science and Technology, University of Macau, Macau, China. Over the past years, he has conducted research on the subjects of navigation guidance and control of air and underwater robots. His current research interests include linear and nonlinear control theory, coordinated control of multiple vehicles, gain scheduled control, integrated design of guidance and control systems, inertial navigation systems, and mission control and real-time architectures for complex autonomous systems with applications to unmanned air and underwater vehicles.

Paulo Oliveira received the Ph.D. degree in electrical and computer engineering from the Instituto Superior Técnico (IST), Lisbon, Portugal, in 2002.

He is currently an Associate Professor with the Department of Mechanical Engineering, IST, and a Researcher with the Institute of Mechanical Engineering, IST. He also collaborates with the Institute for Systems and Robotics, IST. Over the last 25 years, he participated in more than 30 European and Portuguese research projects. He has coauthored more than 200 journal and conference articles. His areas of scientific activity are mechatronics with special focus on the fields of autonomous vehicles, robotics, sensor fusion, navigation, positioning, and nonlinear estimation.